

University of Groningen

## Global 3-D Simulations of the Triple Oxygen Isotope Signature Delta O-17 in Atmospheric CO<sub>2</sub>

Koren, Gerbrand; Schneider, Linda; van der Velde, Ivar R.; van Schaik, Erik; Gromov, Sergey S.; Adnew, Getachew A.; Martino, Dorota J. Mrozek; Hofmann, Magdalena E. G.; Liang, Mao-Chang; Mahata, Sasadhar

*Published in:*  
Journal of geophysical research-Atmospheres

*DOI:*  
[10.1029/2019JD030387](https://doi.org/10.1029/2019JD030387)

**IMPORTANT NOTE:** You are advised to consult the publisher's version (publisher's PDF) if you wish to cite from it. Please check the document version below.

*Document Version*  
Publisher's PDF, also known as Version of record

*Publication date:*  
2019

[Link to publication in University of Groningen/UMCG research database](#)

### *Citation for published version (APA):*

Koren, G., Schneider, L., van der Velde, I. R., van Schaik, E., Gromov, S. S., Adnew, G. A., Martino, D. J. M., Hofmann, M. E. G., Liang, M-C., Mahata, S., Bergamaschi, P., van der Laan-Luijckx, I. T., Krol, M. C., Roeckmann, T., & Peters, W. (2019). Global 3-D Simulations of the Triple Oxygen Isotope Signature Delta O-17 in Atmospheric CO<sub>2</sub>. *Journal of geophysical research-Atmospheres*, 124(15), 8808-8836.  
<https://doi.org/10.1029/2019JD030387>

### **Copyright**

Other than for strictly personal use, it is not permitted to download or to forward/distribute the text or part of it without the consent of the author(s) and/or copyright holder(s), unless the work is under an open content license (like Creative Commons).

The publication may also be distributed here under the terms of Article 25fa of the Dutch Copyright Act, indicated by the "Taverne" license. More information can be found on the University of Groningen website: <https://www.rug.nl/library/open-access/self-archiving-pure/taverne-amendment>.

### **Take-down policy**

If you believe that this document breaches copyright please contact us providing details, and we will remove access to the work immediately and investigate your claim.

## Global 3-D Simulations of the Triple Oxygen Isotope Signature $\Delta^{17}\text{O}$ in Atmospheric $\text{CO}_2$

### Key Points:

- This work presents a first view on possible spatial and temporal gradients of  $\Delta^{17}\text{O}$  in  $\text{CO}_2$  across the globe
- Tropical, boreal, and Southern Hemisphere observations of  $\Delta^{17}\text{O}$  in  $\text{CO}_2$  could be of great interest
- We implemented spatially and temporally explicit sources and sinks of  $\Delta^{17}\text{O}$  in  $\text{CO}_2$  in a 3-D model framework

### Supporting Information:

- Supporting Information S1

### Correspondence to:

G. Koren,  
gerbrand.koren@wur.nl

### Citation:

Koren, G., Schneider, L., van der Velde, I. R., van Schaik, E., Gromov, S. S., Adnew, G. A., et al. (2019). Global 3-D simulations of the triple oxygen isotope signature  $\Delta^{17}\text{O}$  in atmospheric  $\text{CO}_2$ . *Journal of Geophysical Research: Atmospheres*, 124, 8808–8836. <https://doi.org/10.1029/2019JD030387>

Received 1 FEB 2019

Accepted 28 MAY 2019

Accepted article online 19 JUN 2019

Published online 4 AUG 2019

Gerbrand Koren<sup>1</sup>, Linda Schneider<sup>2,3</sup>, Ivar R. van der Velde<sup>4,5</sup>, Erik van Schaik<sup>1</sup>, Sergey S. Gromov<sup>6,7</sup>, Getachew A. Adnew<sup>8</sup>, Dorota J. Mrozek Martino<sup>8</sup>, Magdalena E. G. Hofmann<sup>8,9</sup>, Mao-Chang Liang<sup>10</sup>, Sasadhar Mahata<sup>11</sup>, Peter Bergamaschi<sup>12</sup>, Ingrid T. van der Laan-Luijkx<sup>1</sup>, Maarten C. Krol<sup>1,8</sup>, Thomas Röckmann<sup>8</sup>, and Wouter Peters<sup>1,13</sup>

<sup>1</sup>Meteorology and Air Quality Group, Wageningen University & Research, Wageningen, The Netherlands, <sup>2</sup>Institute of Meteorology and Climate Research (IMK-TRO), Karlsruhe Institute of Technology, Karlsruhe, Germany, <sup>3</sup>Now at Zentrum für Sonnenenergie- und Wasserstoff-Forschung Baden-Württemberg (ZSW), Stuttgart, Germany, <sup>4</sup>Earth System Research Laboratory, National Oceanic and Atmospheric Administration, Boulder, CO, USA, <sup>5</sup>Now at Faculty of Science, VU University Amsterdam, Amsterdam, The Netherlands, <sup>6</sup>Atmospheric Chemistry Department, Max-Planck Institute for Chemistry, Mainz, Germany, <sup>7</sup>Institute of Global Climate and Ecology of Roshydromet and RAS, Moscow, Russia, <sup>8</sup>Institute of Marine and Atmospheric Research, Utrecht University, Utrecht, The Netherlands, <sup>9</sup>Now at Picarro B.V. 's-Hertogenbosch, The Netherlands, <sup>10</sup>Institute of Earth Sciences, Academia Sinica, Taipei, Taiwan, <sup>11</sup>Institute of Global Environmental Change, Xian Jiaotong University, Xian, China, <sup>12</sup>European Commission Joint Research Centre, Ispra (Va), Italy, <sup>13</sup>Centre for Isotope Research, University of Groningen, Groningen, The Netherlands

**Abstract** The triple oxygen isotope signature  $\Delta^{17}\text{O}$  in atmospheric  $\text{CO}_2$ , also known as its “ $^{17}\text{O}$  excess,” has been proposed as a tracer for gross primary production (the gross uptake of  $\text{CO}_2$  by vegetation through photosynthesis). We present the first global 3-D model simulations for  $\Delta^{17}\text{O}$  in atmospheric  $\text{CO}_2$  together with a detailed model description and sensitivity analyses. In our 3-D model framework we include the stratospheric source of  $\Delta^{17}\text{O}$  in  $\text{CO}_2$  and the surface sinks from vegetation, soils, ocean, biomass burning, and fossil fuel combustion. The effect of oxidation of atmospheric CO on  $\Delta^{17}\text{O}$  in  $\text{CO}_2$  is also included in our model. We estimate that the global mean  $\Delta^{17}\text{O}$  (defined as  $\Delta^{17}\text{O} = \ln(\delta^{17}\text{O} + 1) - \lambda_{\text{RL}} \cdot \ln(\delta^{18}\text{O} + 1)$  with  $\lambda_{\text{RL}} = 0.5229$ ) of  $\text{CO}_2$  in the lowest 500 m of the atmosphere is 39.6 per meg, which is ~20 per meg lower than estimates from existing box models. We compare our model results with a measured stratospheric  $\Delta^{17}\text{O}$  in  $\text{CO}_2$  profile from Sodankylä (Finland), which shows good agreement. In addition, we compare our model results with tropospheric measurements of  $\Delta^{17}\text{O}$  in  $\text{CO}_2$  from Göttingen (Germany) and Taipei (Taiwan), which shows some agreement but we also find substantial discrepancies that are subsequently discussed. Finally, we show model results for Zotino (Russia), Mauna Loa (United States), Manaus (Brazil), and South Pole, which we propose as possible locations for future measurements of  $\Delta^{17}\text{O}$  in tropospheric  $\text{CO}_2$  that can help to further increase our understanding of the global budget of  $\Delta^{17}\text{O}$  in atmospheric  $\text{CO}_2$ .

## 1. Introduction

Oxygen has three naturally occurring stable isotopes  $^{16}\text{O}$ ,  $^{17}\text{O}$ , and  $^{18}\text{O}$  of which  $^{16}\text{O}$  is by far the most abundant on Earth. For atmospheric  $\text{CO}_2$ , the relative abundances of  $\text{C}^{16}\text{O}^{16}\text{O}$ ,  $\text{C}^{17}\text{O}^{16}\text{O}$ , and  $\text{C}^{18}\text{O}^{16}\text{O}$  are 99.5%, 0.077%, and 0.41%, respectively (see, e.g., Eiler & Schauble, 2004). We can quantify the oxygen isotopic composition of a sample as

$$\delta^n = \frac{[n\text{O}/^{16}\text{O}]_{\text{sample}}}{[n\text{O}/^{16}\text{O}]_{\text{VSMOW}}} - 1, \quad (1)$$

where  $n$  refers to the rare oxygen isotope (i.e.,  $n = 17$  or  $18$ ) and Vienna Standard Mean Ocean Water (VSMOW) is used as the reference standard and  $\delta$  values are usually expressed in per mil (‰). The isotopic composition of oxygen-containing molecules on Earth, like  $\text{CO}_2$  or  $\text{H}_2\text{O}$ , is affected by processes such as diffusion, evaporation, and condensation. These processes depend on the mass of the molecules and therefore

©2019. The Authors.

This is an open access article under the terms of the Creative Commons Attribution-NonCommercial-NoDerivs License, which permits use and distribution in any medium, provided the original work is properly cited, the use is non-commercial and no modifications or adaptations are made.

result in a mass-dependent fractionation of the oxygen isotopes. As a consequence, the variations in  $\delta^{17}\text{O}$  and  $\delta^{18}\text{O}$  of oxygen-containing substances on Earth are strongly correlated.

A deviation from the mass-dependent fractionation can be expressed by the  $\Delta^{17}\text{O}$  signature (“triple oxygen isotope” or “ $^{17}\text{O}$  excess”). In this study we consistently use the logarithmic definition for  $\Delta^{17}\text{O}$  (see Section S1 of the supporting information for an overview of alternative definitions that are commonly used)

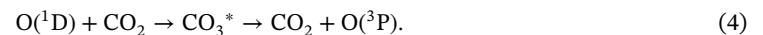
$$\Delta^{17}\text{O} = \ln(\delta^{17}\text{O} + 1) - \lambda_{\text{RL}} \cdot \ln(\delta^{18}\text{O} + 1), \quad (2)$$

which is usually expressed in per mil (‰) or per meg (0.001‰), depending on the magnitude of the  $\Delta^{17}\text{O}$  signature, where  $\lambda_{\text{RL}}$  is the reference line. We selected  $\lambda_{\text{RL}} = 0.5229$ , which is equal to the isotopic equilibration constant of  $\text{CO}_2$  and water  $\lambda_{\text{CO}_2-\text{H}_2\text{O}}$  (Barkan & Luz, 2012), since equilibration of  $\text{CO}_2$  with water is a key process in our study. As a consequence, the  $\Delta^{17}\text{O}$  signature of  $\text{CO}_2$  that equilibrates with a large amount of water will be reset to the  $\Delta^{17}\text{O}$  signature of the water reservoir. Relative to this selected reference line  $\lambda_{\text{RL}}$ , other mass-dependent processes (e.g., diffusion) result in a minor fractionation of oxygen isotopes (fractionation of  $\Delta^{17}\text{O}$  due to diffusion is described in section 2.3.1).

Stratospheric  $\text{CO}_2$  was shown to be anomalously enriched in oxygen isotopes with  $\Delta^{17}\text{O} \gg 0\text{‰}$  in measurement campaigns performed with rockets (Thiemens et al., 1995a), aircraft (Boering et al., 2004; Thiemens et al., 1995b), balloons (Alexander et al., 2001; Kawagucci et al., 2008; Lämmerzahl et al., 2002; Mrozek et al., 2016), or using aircraft and balloons (Wiegel et al., 2013; Yeung et al., 2009). The anomalous isotopic composition of stratospheric  $\text{CO}_2$  has been linked to oxygen exchange with stratospheric  $\text{O}_3$ , which has a positive  $\Delta^{17}\text{O}$  signature, by Yung et al. (1991). Photolysis of  $\text{O}_3$  produces the highly reactive radical  $\text{O}(^1\text{D})$



which can form the unstable  $\text{CO}_3^*$  when colliding with  $\text{CO}_2$ , which dissociates into  $\text{CO}_2$  and an oxygen radical



The oxygen atom that is removed by disintegration of  $\text{CO}_3^*$  is random (except for the small fractionation of a few per mil favoring  $^{18}\text{O}$  remaining in the  $\text{CO}_2$  product; Mebel et al., 2004), such that there is an approximately two-thirds probability that the reactions in equations (3) and (4) will result in the substitution of an oxygen atom in  $\text{CO}_2$  with an oxygen atom that was originally present in  $\text{O}_3$ . This exchange of oxygen atoms from stratospheric  $\text{O}_3$  to  $\text{CO}_2$  is responsible for the transfer of the  $^{17}\text{O}$  anomaly (i.e.,  $\Delta^{17}\text{O} \gg 0\text{‰}$ ) from stratospheric  $\text{O}_3$  to stratospheric  $\text{CO}_2$ .

In the upper troposphere, there is an influx of stratospheric  $\text{CO}_2$  with  $\Delta^{17}\text{O} \gg 0\text{‰}$  (this stratospheric influence on  $\Delta^{17}\text{O}$  of tropospheric  $\text{CO}_2$  was recently observed by Laskar et al. (2019) in air samples from two aircraft flights). Following transport to the troposphere, the  $\text{CO}_2$  is mixed and can come into contact with liquid water in vegetation, soils, or oceans. When  $\text{CO}_2$  dissolves in liquid  $\text{H}_2\text{O}$ , exchange of oxygen atoms occurs, such that the  $\text{CO}_2$  that is released back to the atmosphere has a signature of  $\Delta^{17}\text{O} \approx 0\text{‰}$ . The exchange between  $\text{CO}_2$  and  $\text{H}_2\text{O}$  in vegetation is highly effective due to the presence of the enzyme carbonic anhydrase, whereas the exchange of oxygen isotopes between  $\text{CO}_2$  and cloud droplets is negligible due to the absence of carbonic anhydrase in the atmosphere (Francey & Tans, 1987). The resulting  $\Delta^{17}\text{O}$  signature in tropospheric  $\text{CO}_2$  reflects a dynamic balance of highly enriched stratospheric  $\text{CO}_2$  and equilibration that occurs in vegetation and other water reservoirs. Tropospheric measurements of  $\Delta^{17}\text{O}$  in  $\text{CO}_2$  have previously been performed in Jerusalem, Israel (Barkan & Luz, 2012); La Jolla, United States (Thiemens et al., 2014); Taipei, Taiwan (Liang & Mahata, 2015; Liang et al., 2017a, 2017b; Mahata et al., 2016a), Göttingen, Germany (Hofmann et al., 2017), and Palos Verdes, United States (Liang et al., 2017b).

Gross primary production (GPP; the gross uptake of  $\text{CO}_2$  by vegetation through photosynthesis) is a key process in the carbon cycle which is currently poorly constrained. Increasing our understanding of the terrestrial carbon cycle is essential for predicting future climate and atmospheric  $\text{CO}_2$  concentrations (Booth et al., 2012). An estimate of 120 PgC/year for global GPP was provided by Beer et al. (2010) by using machine learning techniques to extrapolate a database of eddy covariance measurements of  $\text{CO}_2$  to the global domain. An estimate of 150–175 PgC/year for global GPP was derived by Welp et al. (2011) based on the response of

$\delta^{18}\text{O}$  in atmospheric  $\text{CO}_2$  after El Niño–Southern Oscillation events. The large spread in estimates of global GPP clearly indicates our current lack of understanding of the biospheric domain in the global carbon cycle.

Because the  $\Delta^{17}\text{O}$  signature of tropospheric  $\text{CO}_2$  strongly depends on the magnitude of the exchange of  $\text{CO}_2$  with liquid water in leaves, it is a potential tracer for GPP, as was first proposed by Hoag et al. (2005). Similarly, the  $\delta^{18}\text{O}$  signature of tropospheric  $\text{CO}_2$  has been explored to constrain terrestrial carbon fluxes by Ciais et al. (1997a, 1997b), Peylin et al. (1997, 1999), and Cuntz et al. (2003a, 2003b). The main advantage of using  $\Delta^{17}\text{O}$  instead of  $\delta^{18}\text{O}$  is that the signal is less affected by processes in the hydrological cycle (e.g., evaporation and condensation), since these are largely mass dependent (Hoag et al., 2005). Besides constraining gross terrestrial  $\text{CO}_2$  fluxes, other possible applications of  $\Delta^{17}\text{O}$  in atmospheric  $\text{CO}_2$  have been suggested, such as constraining stratospheric circulation and constraining the abundance and variability of  $\text{O}(^1\text{D})$  (e.g., Alexander et al., 2001).

The first two-box model for  $\Delta^{17}\text{O}$  in tropospheric  $\text{CO}_2$  for the Northern and Southern Hemispheres was developed by Hoag et al. (2005). This conceptual box model takes into account the exchange fluxes of  $\text{CO}_2$  between the troposphere and the stratosphere, vegetation, and oceans. In addition, the supply of  $\text{CO}_2$  from fossil fuel combustion and land use change is incorporated in the box model. All these  $\text{CO}_2$  fluxes are associated with a reservoir-specific  $\Delta^{17}\text{O}$  signature. The resulting  $\Delta^{17}\text{O}$  for tropospheric  $\text{CO}_2$  was calculated using a mass balance. Results from Hoag et al. (2005) can be converted into our reference frame, as defined in equation (2), assuming a global  $\delta^{18}\text{O}$  signature of 41.5‰ (observations from Francey & Tans, 1987, show that the global mean  $\delta^{18}\text{O}$  in  $\text{CO}_2$  is  $\sim 0$ ‰ PDB- $\text{CO}_2$ , which can be converted using equation 5 from Brenninkmeijer et al. (1983) into 41.5‰ VSMOW), which yields  $\Delta^{17}\text{O} = 0.066$ ‰ for tropospheric  $\text{CO}_2$ .

A more sophisticated global one-box model was developed by Hofmann et al. (2017). This model takes into account that certain processes (e.g., diffusion of  $\text{CO}_2$  from the atmosphere into leaf stomata) can fractionate oxygen isotopes and influence the  $\Delta^{17}\text{O}$  signature of  $\text{CO}_2$ . Another significant difference with the model from Hoag et al. (2005) is the soil invasion fluxes that are taken into account. Also, both models differ in the magnitude of the  $\text{CO}_2$  fluxes and the  $\Delta^{17}\text{O}$  reservoir signatures. Based on a Monte Carlo simulation where the uncertainty in the input variables is considered, Hofmann et al. (2017) predict  $\Delta^{17}\text{O} = 0.061 \pm 0.033$ ‰ for tropospheric  $\text{CO}_2$ .

In recent years, there have been developments in the available measurement techniques for  $\Delta^{17}\text{O}$  in  $\text{CO}_2$ . Mahata et al. (2013, 2016b) developed a measurement technique based on the equilibration between  $\text{CO}_2$  and  $\text{O}_2$  catalyzed by hot platinum, followed by measurement of the  $\Delta^{17}\text{O}$  signature of  $\text{O}_2$ , from which the initial  $\Delta^{17}\text{O}$  signature of  $\text{CO}_2$  can be inferred with a precision of 8 per meg. Barkan and Luz (2012) developed a high-precision measurement technique based on equilibration of  $\text{CO}_2$  and  $\text{H}_2\text{O}$ , resulting in a precision of 5 per meg for  $\Delta^{17}\text{O}$  in  $\text{CO}_2$ . Using laser-based techniques, Stoltmann et al. (2017) were able to reach a precision for  $\Delta^{17}\text{O}$  in  $\text{CO}_2$  of better than 10 per meg. The quantum cascade laser developed by Aerodyne Research is also able to measure  $\Delta^{17}\text{O}$  in  $\text{CO}_2$  with high precision (McManus et al., 2015; Nelson et al., 2008). In addition, a recently developed ion fragment method allows to measure  $\delta^{17}\text{O}$  and  $\delta^{18}\text{O}$  directly on  $\text{CO}_2$  without the need of chemical conversion (Adnew et al., 2019). The recent developments in the measurement techniques for  $\Delta^{17}\text{O}$  in  $\text{CO}_2$  are essential for its application as tracer for the terrestrial carbon cycle.

Because of the recent advancements in measurement techniques for  $\Delta^{17}\text{O}$  in  $\text{CO}_2$ , it is now possible to observe spatial and temporal gradients of  $\Delta^{17}\text{O}$  more accurately. To simulate the spatial and temporal variability of the  $\Delta^{17}\text{O}$  signal in atmospheric  $\text{CO}_2$ , the available box models are not suitable and a 3-D model framework is required. For this purpose, an oxygen isotope module for atmospheric  $\text{CO}_2$  was implemented in the atmospheric transport model TM5 (Huijnen et al., 2010; Krol et al., 2005). Results from an early version of our 3-D model were compared with the  $\Delta^{17}\text{O}$  measurement series from Göttingen, Germany (Hofmann et al., 2017). A detailed description of our updated  $\Delta^{17}\text{O}$  model is given in section 2, and the changes in our current model with respect to the earlier version used by Hofmann et al. (2017) are summarized in section S2 of the supporting information. The model results are reported in section 3, followed by the discussion and conclusion in sections 4 and 5.

## 2. Methods

### 2.1. General Model Description

Our model framework for  $\Delta^{17}\text{O}$  in atmospheric  $\text{CO}_2$  is based on the atmospheric transport model TM5 (Krol et al., 2005), which is driven by ERA-Interim meteorological fields (Dee et al., 2011) provided by the

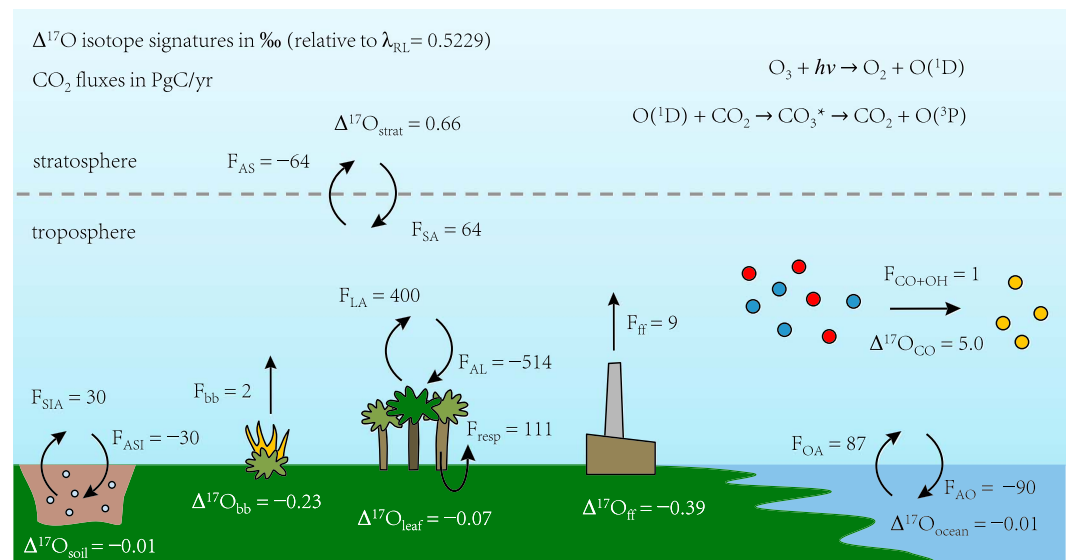


**Figure 1.** Conceptual overview of processes affecting the  $\Delta^{17}\text{O}$  signature of atmospheric  $\text{CO}_2$  in our model. The  $\text{CO}_2$  mass fluxes, indicated with symbol  $F$ , are given in units of  $\text{PgC/year}$ , and  $\Delta^{17}\text{O}$  signatures are given in ‰ as defined in equation (2) relative to a reference line  $\lambda_{\text{RL}} = 0.5229$ . The reported values for  $\text{CO}_2$  mass fluxes are integrated over the global domain, averaged over the years 2012/2013 (as reported in Table S2 of the supporting information) and rounded to integer values. As a sign convention, the  $\text{CO}_2$  mass fluxes that tend to increase the tropospheric  $\text{CO}_2$  mass are expressed as positive numbers. The main source of  $\Delta^{17}\text{O}$  in tropospheric  $\text{CO}_2$  is exchange with the stratosphere ( $F_{\text{SA}}$  and  $F_{\text{AS}}$ ), as described in section 2.2. The stratospheric signature  $\Delta^{17}\text{O}_{\text{strat}}$  in our model is time and space dependent, and the indicated value of  $0.66\text{‰}$  is the effective signature that is associated with stratosphere-troposphere exchange (determined from the stratosphere-troposphere  $\text{CO}_2$  mass flux and  $\Delta^{17}\text{O}$  isoflux as reported in Table S2 of the supporting information). The main sink for  $\Delta^{17}\text{O}$  in tropospheric  $\text{CO}_2$  is the exchange with leaves ( $F_{\text{AL}}$  and  $F_{\text{LA}}$ ), which is associated with a large uncertainty. Also, the magnitude of the exchange fluxes between the soil and atmosphere ( $F_{\text{ASI}}$  and  $F_{\text{SIA}}$ ) is uncertain. The implementation of the surface sources and sinks of  $\text{CO}_2$  is described in section 2.3. Note that the high  $\Delta^{17}\text{O}_{\text{CO}}$  signature is not directly transferred to  $\text{CO}_2$  because of fractionation of oxygen isotopes that occurs during the oxidation of CO, as described in section 2.4.

European Centre for Medium-Range Weather Forecasts. TM5 uses a longitude-latitude grid of  $6^\circ \times 4^\circ$ ,  $3^\circ \times 2^\circ$ , or  $1^\circ \times 1^\circ$  resolution, depending on the chosen setup. Also, TM5 allows the use of two-way nested zoom regions to simulate with a higher horizontal resolution for specific regions. For the vertical coordinate TM5 uses 25, 34, or 60 hybrid sigma-pressure levels, such that the lowest model levels follow the surface elevation and the higher levels are (almost completely) isobaric. For this study, we performed simulations with the coarsest resolution (i.e., a horizontal resolution of  $6^\circ \times 4^\circ$  and 25 vertical levels with the highest model level at 47.8 Pa).

In our model we apply two-way  $\text{CO}_2$  fluxes, exchanging between the stratosphere, biosphere, soil, ocean and the troposphere, and one-way  $\text{CO}_2$  fluxes from fossil fuel combustion, biomass burning, and oxidation of CO into the troposphere, as illustrated in Figure 1. Modeling the gross two-way exchange fluxes for some reservoirs is necessary to estimate the resulting  $\Delta^{17}\text{O}$  signature of tropospheric  $\text{CO}_2$ . The  $\text{CO}_2$  fluxes in our model are time and space dependent and can originate from the stratosphere (described in section 2.2), the Earth surface (section 2.3) and are present within the troposphere itself in the case of oxidation of atmospheric CO (section 2.4). Also, the  $\Delta^{17}\text{O}$  signatures of the different reservoirs are indicated in Figure 1. The  $\Delta^{17}\text{O}$  signatures for stratospheric  $\text{CO}_2$ , soil water, leaf water, and atmospheric CO are time and space dependent in our model. Note that for the exchange fluxes between the atmosphere and biosphere, kinetic fractionation affects the  $\Delta^{17}\text{O}$  signature (described in sections 2.3.1 and 2.3.2) and that the oxidation of CO by OH is not a mass-dependent process, such that the  $\Delta^{17}\text{O}$  signature of atmospheric CO is not directly transferred to  $\text{CO}_2$  (described in more detail in section 2.4).

In our model framework we implemented  $\text{CO}_2$  and  $\text{C}^{17}\text{OO}$  as independent tracers, while assuming a fixed atmospheric signature of  $\delta^{18}\text{O} = 41.5\text{‰}$  VSMOW. With the fixed  $\delta^{18}\text{O}$ , we can translate the imposed boundary conditions (i.e., sources and sinks) of  $\Delta^{17}\text{O}$  into an equivalent boundary condition for the  $\delta^{17}\text{O}$  signature, based on equation (2). Subsequently, the  $\text{C}^{17}\text{OO}$  tracer mass can be determined from the local tracer mass



**Table 1**  
Overview of the Main Model Parameters and Available Settings for the 3-D  $\Delta^{17}\text{O}$  Model

Reservoir	Section	Model parameter	Base setting	Alternative settings
Stratosphere	2.2	$\Delta^{17}\text{O}\text{--}\text{N}_2\text{O}$ fit	Least squares fit	Upper/lower 95% confidence limit fit
		$[\text{N}_2\text{O}]$ fit threshold	240 ppb level	Zero or positive value
		Relaxation time scale	0 hr (i.e., no relaxation)	Zero or positive value
Vegetation	2.3.1	Soil water $\Delta^{17}\text{O}$	Distributed from precipitation	Constant $\Delta^{17}\text{O}_{\text{soil}}$
		Leaf water $\Delta^{17}\text{O}$	Dynamic from rel. humidity	Constant $\lambda_{\text{transp}}$
Soil	2.3.2	Invasion flux magnitude	30 PgC/year globally	Zero or positive value
		Invasion flux distribution	Scaled from $\text{CO}_2$ respiration flux	Scaled from $\text{H}_2$ deposition velocity
Ocean	2.3.3	$\text{CO}_2$ fluxes	Dynamically coupled to $[\text{CO}_2]$	Calculated from predefined $[\text{CO}_2]$
		$\text{C}^{17}\text{OO}$ fluxes	Dynamically coupled to $[\text{C}^{17}\text{OO}]$	Calculated from predefined $[\text{C}^{17}\text{OO}]$
Atmospheric $\text{CO}$	2.4	Setting	Not included	Included with nonzero $\epsilon_{\text{CO+OH}}$

*Note.* Note that the soil water signature  $\Delta^{17}\text{O}_{\text{soil}}$  is listed here under the vegetation reservoir, but it also affects the soil invasion fluxes. The model results with base settings are described in sections 3.1.1 and 3.1.2. The effect of some of the alternative settings on the model predictions is discussed in section 3.1.3.

of  $\text{CO}_2$  and  $\delta^{17}\text{O}$  using equation (1). The  $\text{C}^{17}\text{OO}$  tracer mass can then be transported in our atmospheric model. By again using  $\delta^{18}\text{O} = 41.5\text{‰}$  VSMOW, we can “translate” the simulated  $\text{C}^{17}\text{OO}$  tracer mass back into  $\Delta^{17}\text{O}$  for analysis. By using a fixed  $\delta^{18}\text{O}$  signature, we are able to simulate the transport of the  $\Delta^{17}\text{O}$  signature in  $\text{CO}_2$ , without the need of explicitly modeling the variations in  $\delta^{18}\text{O}$  that are strongly related to the water cycle (Ciais et al., 1997a, 1997b; Cuntz et al., 2003a, 2003b; Peylin et al., 1997, 1999). The consequence of this approach is that our model simulated  $\delta^{17}\text{O}$  cannot be directly compared to  $\delta^{17}\text{O}$  observations. Model output becomes meaningful after converting the simulated  $\delta^{17}\text{O}$  fields using the fixed  $\delta^{18}\text{O}$  signature into  $\Delta^{17}\text{O}$  fields. To convert isotopic signatures to isotope ratios, we use  $[\text{O}^{18}/\text{O}^{16}]_{\text{VSMOW}} = 2005.20 \cdot 10^{-6}$  (Baertschi, 1976) and  $[\text{O}^{17}/\text{O}^{16}]_{\text{VSMOW}} = 379.9 \cdot 10^{-6}$  (Li et al., 1988). Note that more recent studies estimate the latter to be slightly higher,  $386.7 \cdot 10^{-6}$  and  $382.7 \cdot 10^{-6}$  according to Assonov and Brenninkmeijer (2003) and Kaiser (2008) respectively, but the effect on our simulated  $\Delta^{17}\text{O}$  is negligible.

We have defined several model parameters that can be set to user-specified values. The motivation for this implementation is that many of the model parameters are uncertain (e.g., the magnitude of the soil invasion flux, as discussed in section 2.3.2), and this flexibility allows us to efficiently investigate the sensitivity to these model parameters. An overview of the most important model parameters and the available settings is given in Table 1. A more detailed explanation of the model parameters and available settings is given in the

**Table 2**  
Overview of Performed Simulations for Sensitivity Analysis Including the Base Model Run

Name	Description
BASE	Base model run
ST_LOWER	95% confidence interval lower limit fit
ST_UPPER	95% confidence interval upper limit fit
SOIL_CONST	$\Delta^{17}\text{O}_{\text{soil}} = -5$ per meg
LEAF_CONST	$\lambda_{\text{transp}} = 0.5156$
RESP_240	Respiration scaling; global magnitude 240 PgC/year
RESP_450	Respiration scaling; global magnitude 450 PgC/year
HYD_240	$\text{H}_2$ deposition scaling; global magnitude 240 PgC/year
HYD_450	$\text{H}_2$ deposition scaling; global magnitude 450 PgC/year
CO_ROCK	$\epsilon_{\text{CO+OH}}$ from Röckmann et al. (1998a)
CO_FEIL	$\epsilon_{\text{CO+OH}}$ from Feilberg et al. (2005)

*Note.* The resulting  $\Delta^{17}\text{O}$  signature of atmospheric  $\text{CO}_2$  and the  $\Delta^{17}\text{O}$  isofluxes for the base model run are discussed in sections 3.1.1 and 3.1.2. The results of the sensitivity analyses are given in section 3.1.3.

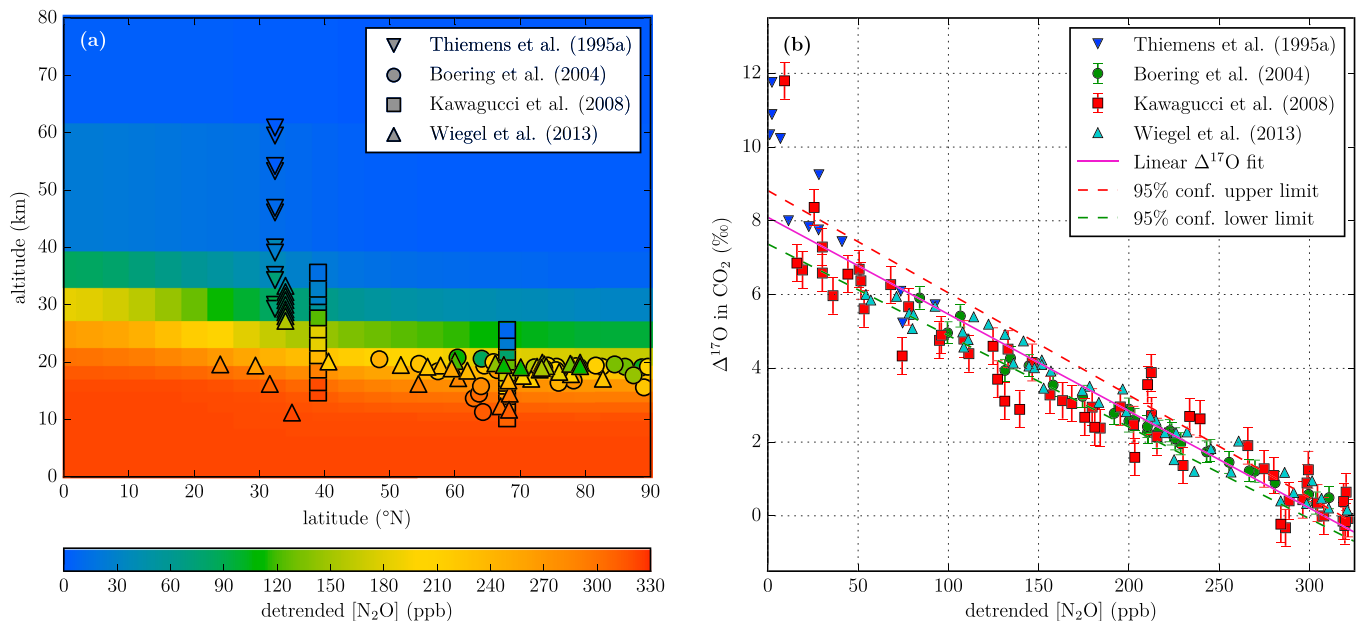


**Figure 2.** Overview of simulated and measured stratospheric  $N_2O$  mole fraction and  $\Delta^{17}O$  signature in  $CO_2$ . (a) Annual mean, zonal mean TM5 model predictions of detrended  $N_2O$  mole fractions using a horizontal resolution of  $6^\circ \times 4^\circ$  and 25 vertical levels compared to detrended measurements of  $N_2O$  mole fractions from Thiemens et al. (1995a), Boering et al. (2004), Kawagucci et al. (2008), and Wiegel et al. (2013) for stratospheric air in Northern Hemisphere. The background color indicates the value of the TM5 model prediction, and the color of the symbols indicates the measured value. (b)  $\Delta^{17}O$  signatures of stratospheric  $CO_2$  versus detrended  $N_2O$  mole fraction, constructed from measurements by Thiemens et al. (1995a), Boering et al. (2004), Kawagucci et al. (2008), and Wiegel et al. (2013) and linear least squares fit with its corresponding 95% confidence interval. The error bars from Thiemens et al. (1995a) and Wiegel et al. (2013) are omitted from the figure to improve visibility.

following sections. A summary of the model simulations that were conducted in this research is provided in Table 2.

## 2.2. Stratospheric Source of $\Delta^{17}O$ in $CO_2$

### 2.2.1. $N_2O$ – $\Delta^{17}O(CO_2)$ Correlation

The production of isotopically anomalously enriched  $CO_2$  in the stratosphere has been linked to the exchange of oxygen atoms between  $O_3$  and  $CO_2$  via  $O(^1D)$  as described in section 1 and shown in equations (3) and (4). Since the initial discovery of stratospheric  $CO_2$  with  $\Delta^{17}O \gg 0\text{‰}$ , a number of research groups were able to produce anomalously enriched  $CO_2$  from UV-irradiated  $O_2$  or  $O_3$  and  $CO_2$  in controlled laboratory environments (Chakraborty & Bhattacharya, 2003; Johnston et al., 2000; Shaheen et al., 2007; Wen & Thiemens, 1993; Wiegel et al., 2013). Despite the knowledge gained through these studies, there are currently still many questions remaining regarding the dependence on temperature, pressure, photolysis wavelength, and concentrations of  $O_2$ ,  $O_3$ , and  $CO_2$  in the stratosphere. Considering the uncertainties associated with explicitly modeling the production of  $\Delta^{17}O$  in  $CO_2$  based on the reactions in equations (3) and (4), we decided to impose  $\Delta^{17}O$  in stratospheric  $CO_2$  based on its observed correlation with  $N_2O$ , which we expect to be a more robust approach.

The correlation between  $N_2O$  and  $\Delta^{17}O$  in  $CO_2$  was first used by Luz et al. (1999) to estimate the stratospheric influx of  $\Delta^{17}O$  for  $CO_2$  and  $O_2$  into the troposphere. Boering et al. (2004) describe that atmospheric transport is the physical mechanism behind the  $N_2O$ – $\Delta^{17}O(CO_2)$  correlation, as both  $N_2O$  and  $\Delta^{17}O$  in  $CO_2$  are long-lived tracers (the lifetime of  $N_2O$  is approximately 120 years; Volk et al., 1997). The negative slope of the  $N_2O$ – $\Delta^{17}O(CO_2)$  correlation is explained by the opposite effect of stratospheric photochemistry on  $N_2O$  and  $\Delta^{17}O$  in  $CO_2$  ( $\Delta^{17}O$  in  $CO_2$  is produced from  $O(^1D)$  originating from  $O_3$  photolysis, as described in section 1, and  $N_2O$  is removed by photolysis and  $O(^1D)$ , as described in section 2.2.2).

Experimental data sets for stratospheric  $N_2O$  and  $\Delta^{17}O$  in  $CO_2$  from Thiemens et al. (1995a), Boering et al. (2004), Kawagucci et al. (2008), and Wiegel et al. (2013) were examined to test the robustness of the  $N_2O$ – $\Delta^{17}O(CO_2)$  correlation. The  $\Delta^{17}O$  values for these studies were recalculated from the reported  $\delta^{17}O$  and  $\delta^{18}O$  signatures using the definition of  $\Delta^{17}O$  as given in equation (2). The  $N_2O$  mole fractions were detrended to account for the atmospheric growth rate of  $N_2O$  and the difference in date of sample collection,

according to the detrending procedure described in section 2.2.2. The reader is referred to the original works for details on experimental techniques and the associated uncertainties. Despite the difference in date and location of sample collection, there is a strong correlation between the  $\text{N}_2\text{O}$  mole fraction and the  $\Delta^{17}\text{O}$  signature of  $\text{CO}_2$  that is linear for  $\text{N}_2\text{O}$  in the range of 50 to 320 ppb as shown in Figure 2b. In the mesosphere the correlation between  $\text{N}_2\text{O}$  and  $\Delta^{17}\text{O}$  in  $\text{CO}_2$  breaks down as discussed in detail by Mrozek (2017).

We derived a linear fit for the detrended  $\text{N}_2\text{O}$  mole fraction and  $\Delta^{17}\text{O}$  in  $\text{CO}_2$  using a least squares approach with equal weights assigned to each individual measurement (data for  $[\text{N}_2\text{O}] < 50$  ppb was excluded), based on the formulation

$$\Delta^{17}\text{O}_{\text{fit}} = a \cdot ([\text{N}_2\text{O}]_{\text{dtd}} - 320.84) + b, \quad (5)$$

where  $[\text{N}_2\text{O}]_{\text{dtd}}$  is the detrended  $\text{N}_2\text{O}$  mole fraction. In addition to the least squares solution for the coefficients  $a$  and  $b$  in equation (5), we also constructed a 95% confidence interval, as shown in Figure 2b. The effect of the  $\text{N}_2\text{O}$ – $\Delta^{17}\text{O}$  fit on the resulting distribution of  $\Delta^{17}\text{O}$  in  $\text{CO}_2$  is tested by performing different simulations (BASE, ST\_UPPER and ST\_LOWER as defined in Table 2), the results of which are discussed in section 3.1.3.

In our model framework, the fit in equation (5) is implemented with a cutoff at 0‰, to prevent negative  $\Delta^{17}\text{O}$  values in the stratosphere. Also, a relaxation time can be specified in the model that determines the strength of the coupling between  $\Delta^{17}\text{O}$  for stratospheric  $\text{CO}_2$  and  $\text{N}_2\text{O}$  mole fractions, such that

$$\Delta^{17}\text{O}_{\text{new}} = \Delta^{17}\text{O}_{\text{fit}} + e^{-\Delta t/\tau_{\text{relax}}}(\Delta^{17}\text{O}_{\text{old}} - \Delta^{17}\text{O}_{\text{fit}}), \quad (6)$$

where  $\Delta t$  is the model time step,  $\tau_{\text{relax}}$  is a user-specified time scale, and  $\Delta^{17}\text{O}_{\text{new}}$  and  $\Delta^{17}\text{O}_{\text{old}}$  refer to  $\Delta^{17}\text{O}$  signature for the new and old time steps, respectively. In our model, we can apply the fit based on the vertical level (e.g., for cells with atmospheric pressure below 100 hPa) or depending on the local  $\text{N}_2\text{O}$  mole fraction (e.g., for cells with  $\text{N}_2\text{O}$  mole fractions below 280 ppb). The values used for these parameters in the base model run are summarized in Table 1.

### 2.2.2. $\text{N}_2\text{O}$

We simulated  $\text{N}_2\text{O}$  based on stratospheric sinks and optimized surface fluxes from Corazza et al. (2011) and Bergamaschi et al. (2015). The 2-D surface fluxes have a time resolution of 1 month and a horizontal resolution of  $6^\circ \times 4^\circ$ . The 3-D sink fields have the same time resolution and same horizontal resolution and consist of 25 vertical levels. The  $\text{N}_2\text{O}$  surface fluxes are optimized for the years 2006 and 2007 by Corazza et al. (2011) and Bergamaschi et al. (2015), and we extrapolate the  $\text{N}_2\text{O}$  sources for years outside of this range. The  $\text{N}_2\text{O}$  sinks are climatological fields derived from the ECHAM5/MESSy1 model (Brühl et al., 2007). The sink fields distinguish between  $\text{N}_2\text{O}$  loss caused by  $\text{O}(^1\text{D})$  (roughly 10% of total loss) and photolysis (roughly 90% of  $\text{N}_2\text{O}$  loss) and have a strong seasonal cycle due to the changing orientation of the Earth with respect to the Sun. The sum of the yearly emissions is on average:  $\sim 16$  TgN/year, and the imbalance between the sources and sinks is  $\sim 3.5$  TgN/year, resulting in an increase of the  $\text{N}_2\text{O}$  mass in our model. The global  $\text{N}_2\text{O}$  emission and growth rate are in good agreement with results from Hirsch et al. (2006).

In this study, we are not interested in the atmospheric increase of the  $\text{N}_2\text{O}$  mole fraction over time but its correlation with  $\Delta^{17}\text{O}$  in  $\text{CO}_2$ . Assonov et al. (2013) have encountered the same issue and constructed a detrending method based on measured  $\text{N}_2\text{O}$  at Mauna Loa. This detrending method assumes a constant growth rate for  $\text{N}_2\text{O}$  mole fractions of  $\alpha_{\text{ref}} = 0.844 \pm 0.001$  ppb/year, which is representative of tropospheric air but not suitable to the (upper) stratospheric air that we also consider in this study (e.g., upper stratospheric air samples from Thieme et al. (1995a) with  $\text{N}_2\text{O}$  mole fractions of less than 10 ppb). We modified the detrending method from Assonov et al. (2013) as described in section S3 of the supporting information to arrive at

$$X_{\text{dtd}} = X_{\text{obs}} \cdot \left[ 1 - \frac{\alpha_{\text{ref}}}{X_{\text{ref}}} \cdot (t_{\text{ref}} - t_{\text{obs}}) \right]^{-1}, \quad (7)$$

where  $X_{\text{obs}}$  and  $X_{\text{dtd}}$  refer to the observed and detrended mole fractions and where  $t_{\text{obs}}$  and  $t_{\text{ref}}$  are, respectively, the time of observation and the reference time (1 January 2007) on which the  $\text{N}_2\text{O}$  mole fractions are projected. This detrending scheme is applied for (1) the validation of the  $\text{N}_2\text{O}$  simulation against  $\text{N}_2\text{O}$  observations, (2) the derivation of the  $\text{N}_2\text{O}$ – $\Delta^{17}\text{O}$  fit, and (3) the detrending of simulated stratospheric  $\text{N}_2\text{O}$  before applying the correlation in TM5.



The modeled tropospheric N<sub>2</sub>O mole fraction is nearly constant (well mixed) at ~320 ppb (for 1 January 2007), and the NH mole fraction is roughly 0.7–1 ppb higher than for the SH, which agrees well with the results from Hirsch et al. (2006). To test the uncertainty that is associated with our modeled N<sub>2</sub>O, we compare our model predictions for N<sub>2</sub>O with stratospheric measurements of N<sub>2</sub>O. Figure 2a shows a comparison of modeled zonal mean, yearly mean N<sub>2</sub>O with detrended experimental data from Thiemens et al. (1995a), Boering et al. (2004), Kawagucci et al. (2008), and Wiegel et al. (2013). For the measurements from Thiemens et al. (1995a), we assume that the latitude of measurements is equal to latitude of the launching site of the rocket. Our model prediction agrees well with the vertical profile from Kawagucci et al. (2008) at 39°N but overestimates the N<sub>2</sub>O mole fractions in the upper part of the vertical profile at 68°N. In Figure S1 of the supporting information we provide similar plots for each season.

### 2.2.3. Stratosphere-Troposphere Exchange

The transport of air masses in our model, including stratosphere-troposphere exchange (STE), is fully driven by the European Centre for Medium-Range Weather Forecasts ERA-Interim meteorological fields (Dee et al., 2011). Since STE is essential in this study, both for the transport of N<sub>2</sub>O and for CO<sub>2</sub> with anomalous  $\Delta^{17}\text{O}$ , we aim to diagnose the magnitude and variability of STE. The diagnosed spatiotemporal variation of STE could help to explain variations in predicted  $\Delta^{17}\text{O}$  in the troposphere.

To diagnose the STE of CO<sub>2</sub> in TM5, two artificial tracers were defined: CO2\_trop and CO2\_strat that have the same properties as the normal tracer CO<sub>2</sub> but do not have any sources or sinks at the surface. For each time step, the tracer mass and tracer mass slopes of CO2\_trop in tropospheric cells are copied from CO<sub>2</sub>, whereas the tracer mass and slopes of CO2\_trop are set equal to zero for all stratospheric cells. The opposite procedure is performed each time step for the tracer CO2\_strat after which all tracers in the model are transported. By diagnosing the tracer mass of CO2\_trop that was transported into the stratosphere, we can determine for each time step a 2-D field of the transport across the user-defined tropopause. By combining the two gross exchange fluxes from CO2\_trop and CO2\_strat, we can calculate the net STE flux. This method allows the use of a static flat “tropopause” or a dynamic tropopause derived from the local temperature profile or the local N<sub>2</sub>O mole fraction. The transport of C<sup>17</sup>OO is tracked in a similar fashion, which allows for the calculation of the  $\Delta^{17}\text{O}$  stratospheric isoflux. Finally, we can determine the troposphere-stratosphere flux  $F_{AS}$  by integrating over the tropical region (30°S to 30°N) and the stratosphere-troposphere flux  $F_{SA}$  by integrating over the extratropical regions (outside the range 30°S to 30°N).

It is known that meteorological fields from data assimilation systems have the tendency to overestimate the Brewer-Dobson circulation (Bregman et al., 2006; van Noije et al., 2004). The ERA-Interim reanalysis performs better at simulating the Brewer-Dobson circulation than its predecessor ERA-40 (Monge-Sanz et al., 2007), but upward transport is still too large compared to observations (Schoeberl et al., 2008). Also, the advection scheme for transport of tracer mass has an effect on the STE. Bönisch et al. (2008) showed that the “second-order moments” scheme (Prather, 1986) is more accurate for stratospheric transport than the “slopes” scheme by Russell and Lerner (1981) that is used in our current model framework.

Given the importance of STE for our purposes and the difficulty of accurately modeling STE, we compared our diagnosed STE with data from Appenzeller et al. (1996) and Holton (1990). These studies were also used by Luz et al. (1999) to calculate the stratospheric source of  $\Delta^{17}\text{O}$  for tropospheric CO<sub>2</sub> and O<sub>2</sub> and in the box models by Hoag et al. (2005) and Hofmann et al. (2017). In order to determine the air mass flux crossing the tropopause, we switched off the CO<sub>2</sub> sources and sinks at the surface and initialized the CO<sub>2</sub> tracer with a constant mixing ratio throughout the entire domain. Using our method to track the STE of CO<sub>2</sub> and the imposed constant CO<sub>2</sub> mixing ratio, we inferred the air mass STE. The comparison of our derived STE and data from Appenzeller et al. (1996) and Holton (1990) is shown in Figure 3. It should be noted that the pressure levels for which the fluxes are given are not equal and also the years are different (as indicated in the legend). Still, some general conclusions about the STE in TM5 can be made. The magnitude of the STE from TM5 is for most months in between the estimates from Appenzeller et al. (1996) and Holton (1990) and the timing of the seasonality in STE agrees well. Despite the agreement, it should be noted that the range of reported values by Appenzeller et al. (1996) and Holton (1990) is large, and hence, considerable uncertainty is associated with our model derived STE. The implications of the large uncertainty in STE on the potential application of  $\Delta^{17}\text{O}$  in CO<sub>2</sub> as tracer of GPP are further discussed in section 4.3.

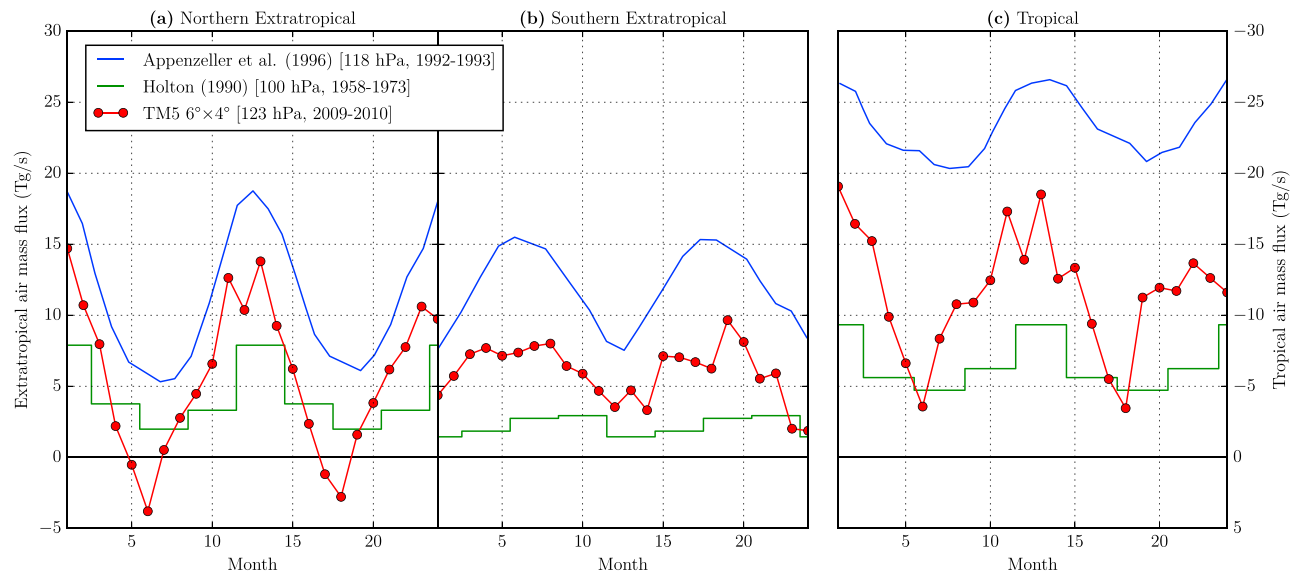


**Figure 3.** Net air mass flux through  $\sim 100$ -hPa pressure levels from TM5 model simulation and from literature for two consecutive years. Mass fluxes from Appenzeller et al. (1996) for years 1992–1993 are given for the 118-hPa surface. Mass fluxes from Holton (1990) are averaged over years 1958–1973; this averaged data are shown for the first years and are repeated for the second year. Monthly output was taken from our TM5 model simulation; the predicted mass flux is given for 123 hPa for years 2009 and 2010. (a) Fluxes for northern extratropical region (latitudes above  $30^\circ\text{N}$ ). (b) Fluxes for southern extratropical region (latitudes below  $30^\circ\text{S}$ ). (c) Fluxes for tropical region (latitudes between  $30^\circ\text{N}$  and  $30^\circ\text{S}$ ). Note that for the tropical mass flux the vertical axis is shown on the right-hand side of the figure and is reversed to facilitate easy visual comparison with the extratropical regions.

The mass fluxes from Appenzeller et al. (1996) are derived from the U.K. Meteorological Office data set (Swinbank & O'Neill, 1994) with a resolution of  $3.75^\circ$  longitude by  $2.5^\circ$  latitude and with a vertical resolution of  $\sim 50$  hPa in the lowermost stratosphere. We reproduced the STE graph by carefully extracting data points from the graphs in Appenzeller et al. (1996). STE mass fluxes by Holton (1990) are derived from climatological data of Oort (1983) specified on  $5^\circ$  latitude intervals and aggregated for the different seasons. Our TM5 simulation was performed with a horizontal resolution of  $6^\circ \times 4^\circ$  and for 25 vertical levels. The TM5 model uses hybrid sigma-pressure levels; for the level at which the mass flux is diagnosed, the levels are almost completely isobaric.

### 2.3. Surface Sinks of $\Delta^{17}\text{O}$ in $\text{CO}_2$

#### 2.3.1. Atmosphere-Leaf Exchange

The atmosphere-leaf exchange of  $\text{CO}_2$  is modeled using the Simple Biosphere/Carnegie-Ames-Stanford Approach (SiBCASA) model (Schaefer et al., 2008). To calculate photosynthesis, SiBCASA combines the  $\text{C}_3$  and  $\text{C}_4$  assimilation models (Collatz et al., 1992; Farquhar et al., 1980) with the Ball-Berry-Collatz stomatal conductance model (Collatz et al., 1991), from which the internal leaf  $\text{CO}_2$  concentration  $c_i$  can be calculated. SiBCASA is driven by ERA-Interim meteorology with 3-hourly time resolution and a spatial resolution of  $1^\circ \times 1^\circ$ . Furthermore, the spatial distribution of  $\text{C}_3$  and  $\text{C}_4$  vegetation is taken from Still et al. (2003) and SiBCASA uses a climatological mean seasonal leaf phenology based on satellite-derived Normalized Difference Vegetation Index. SiBCASA results are first stored in full resolution in files that are subsequently read by our atmospheric transport model TM5.

The gross atmosphere-leaf exchange fluxes can be derived from the ratio of leaf internal to atmospheric  $\text{CO}_2$  concentration  $c_i/c_a$  and the assimilation flux  $F_A$  (which we obtain by scaling GPP with a factor 0.88, to take out the component that is released through autotrophic leaf respiration, similar to Ciais et al., 1997a), according to

$$F_{\text{AL}} = F_A \frac{c_a}{c_a - c_i}, \quad F_{\text{LA}} = -F_A \frac{c_i}{c_a - c_i}. \quad (8)$$

We have used monthly averaged GPP-weighted  $c_i/c_a$  ratios, similar to Ciais et al. (1997a, 1997b) and Peylin et al. (1997, 1999). Furthermore, our assimilation flux has 3-hourly time resolution, whereas we assume that leaf respiration is a constant fraction of GPP. In future studies we recommend to include  $c_i/c_a$  and leaf

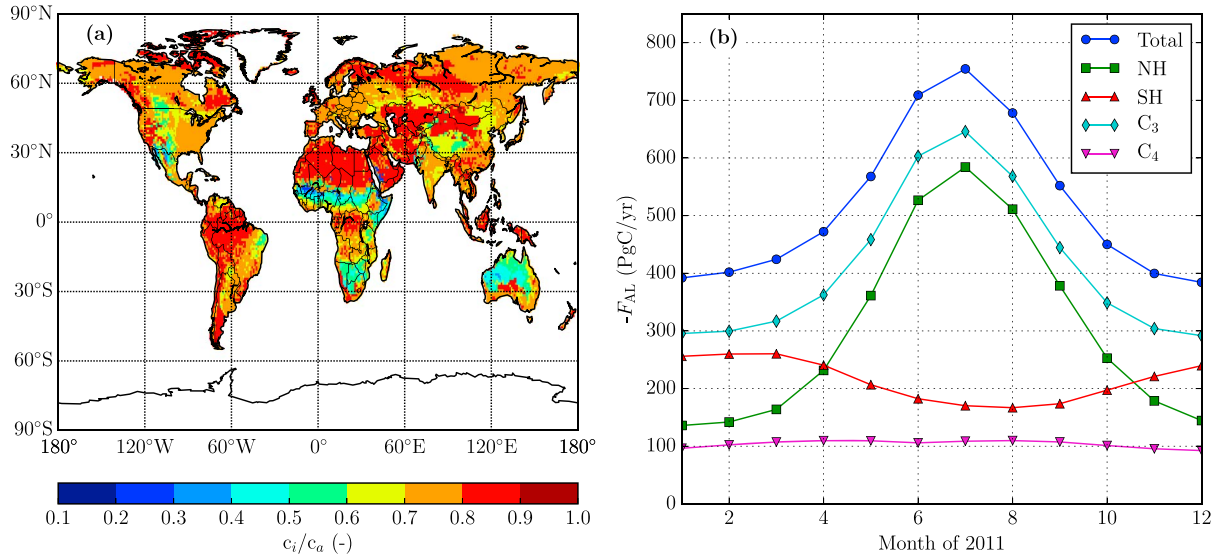


**Figure 4.** Vegetation parameters as predicted by Simple Biosphere/Carnegie-Ames-Stanford Approach (SiBCASA). (a) Spatial distribution of gross primary production weighted  $c_i/c_a$  over the Earth surface averaged over the year 2011. (b) Temporal variation of global atmosphere-leaf flux  $F_{AL}$  as predicted by SiBCASA, partitioned over Northern Hemisphere (NH)/Southern Hemisphere (SH) and for  $C_3/C_4$  vegetation.

respiration at the same temporal resolution as GPP, similar to the model by Cuntz et al. (2003a, 2003b) for  $\delta^{18}\text{O}$  in  $\text{CO}_2$ , as is also discussed in section 4.1.

In our model framework, we use the sign convention that positive fluxes increase the  $\text{CO}_2$  mass in the troposphere. The magnitude of global GPP in our model is taken from SiBCASA and is  $-133 \text{ PgC/year}$  for 2011. This represents a larger uptake than the values of  $-100$  and  $-120 \text{ PgC/year}$  as used in the box models by Hoag et al. (2005) and Hofmann et al. (2017), respectively.

The average distribution of GPP-weighted  $c_i/c_a$  for 2011 and the resulting gross atmosphere-leaf flux  $F_{AL}$  are shown in Figure 4. The presence of  $C_4$  vegetation in tropical Africa can be recognized clearly by the band of relatively low  $c_i/c_a$  ratios near the equator. Our  $c_i/c_a$  ratios are higher than what was used in the box models by Hofmann et al. (2017) (a fixed ratio of 0.7) and Hoag et al. (2005) (two thirds and one third for  $C_3$  and  $C_4$  vegetation, respectively, based on a study by Pearcy & Ehleringer, 1984). To prevent excessive atmosphere leaf fluxes in our model, we have imposed an upper limit such that  $c_i/c_a \leq 0.9$  for all grid cells in the domain during all months of the simulation. Our global gross atmosphere-leaf fluxes in Figure 4b exhibit a clear seasonal signal, peaking during the NH summer months. During the entire year, our atmosphere-leaf flux is larger than the estimated  $-352 \text{ PgC/year}$  from the box model by Hofmann et al. (2017), which can be explained by our higher  $c_i/c_a$  ratios and the larger magnitude of our assimilation flux  $F_A$ .

A fraction of the  $\text{CO}_2$  that diffuses out of the leaf has equilibrated with leaf water inside the leaf. This can be expressed by dividing the gross leaf-atmosphere flux  $F_{AL}$  into an equilibrated and nonequilibrated part

$$F_{LAeq} = (f_{C_3} \cdot \theta_{C_3} + f_{C_4} \cdot \theta_{C_4}) \cdot F_{LA}, \quad (9)$$

$$F_{LANeq} = (f_{C_3} \cdot [1 - \theta_{C_3}] + f_{C_4} \cdot [1 - \theta_{C_4}]) \cdot F_{LA}, \quad (10)$$

where  $f_{C_i}$  refers to the fraction of a vegetation type and  $\theta_{C_i}$  is the vegetation type-specific equilibration constant. In our model we use  $\theta_{C_3} = 0.93$  and  $\theta_{C_4} = 0.38$  (Gillon & Yakir, 2000, 2001).

The isotopic signature associated with the gross atmosphere-leaf exchange fluxes is determined by the signature of the source (atmospheric  $\text{CO}_2$  for  $F_{AL}$  and  $F_{LANeq}$  and leaf water for  $F_{LAeq}$ ) and kinetic fractionation during inflow and outflow of  $\text{CO}_2$  through the leaf stomata

$$\Delta^{17}\text{O}_{AL} = \Delta^{17}\text{O}_A + (\lambda_{\text{kinetic}} - \lambda_{\text{RL}}) \cdot \ln(\alpha_{\text{leaf}}), \quad (11)$$

$$\Delta^{17}\text{O}_{LAeq} = \Delta^{17}\text{O}_{\text{leaf}} + (\lambda_{\text{kinetic}} - \lambda_{\text{RL}}) \cdot \ln(\alpha_{\text{leaf}}), \quad (12)$$

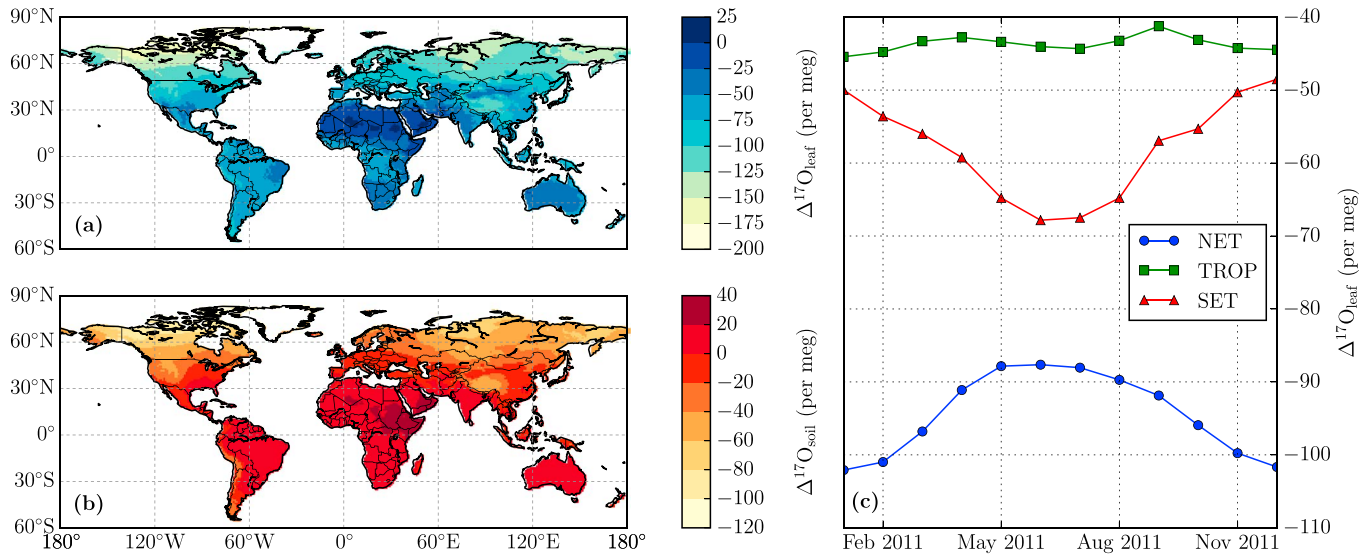


**Figure 5.**  $\Delta^{17}\text{O}$  signature of soil water and leaf water. (a) Annual mean distribution of  $\Delta^{17}\text{O}_{\text{leaf}}$  for 2011. (b) Annual mean distribution of  $\Delta^{17}\text{O}_{\text{soil}}$  for 2011. (c) Temporal variation of  $\Delta^{17}\text{O}_{\text{leaf}}$  for northern extratropical region (NET; latitudes above  $30^\circ\text{N}$ ), tropical region (TROP; latitudes between  $30^\circ\text{S}$  and  $30^\circ\text{N}$ ), and southern extratropical region (SET; latitudes below  $30^\circ\text{S}$ ) during 2011.

$$\Delta^{17}\text{O}_{\text{LAnoneq}} = \Delta^{17}\text{O}_A + (\lambda_{\text{kinetic}} - \lambda_{\text{RL}}) \cdot \ln(\alpha_{\text{leaf}}), \quad (13)$$

where  $\Delta^{17}\text{O}_A$  and  $\Delta^{17}\text{O}_{\text{leaf}}$  are the  $\Delta^{17}\text{O}$  signatures for atmospheric  $\text{CO}_2$  and for  $\text{CO}_2$  that has equilibrated with leaf water,  $\alpha_{\text{leaf}} = 0.9926$  is the fractionation factor for diffusion of  $\text{C}^{18}\text{OO}$  relative to  $\text{CO}_2$  through leaf stomata (Farquhar et al., 1993), and  $\lambda_{\text{kinetic}} = 0.509$  is the coefficient associated with kinetic fractionation of  $\text{C}^{17}\text{OO}$  relative to  $\text{C}^{18}\text{OO}$  (Young et al., 2002). A derivation and process-based interpretation of equation (11) is given in section S4 of the supporting information. An alternative derivation for equations (11)–(13) is given in section S5 of the supporting information.

To calculate  $\Delta^{17}\text{O}_{\text{leaf}}$ , we first need to determine the isotopic signature of soil water  $\Delta^{17}\text{O}_{\text{soil}}$ . We derive the  $\delta^{18}\text{O}$  signature of soil water from the  $\delta^{18}\text{O}$  signature of precipitation water, which we obtained from Bowen and Revenaugh (2003) through the portal <http://www.waterisotopes.org>. We use the yearly average precipitation water signatures, since the amplitude in the seasonal signal of soil water is weaker than for precipitation water and the phase of the seasonal signal can be shifted depending on the depth of the soil water in the soil layer (e.g., Affolter et al., 2015). Similar to Hofmann et al. (2017), we derive the  $\Delta^{17}\text{O}$  signature of soil water from its  $\delta^{18}\text{O}$  signature by assuming that soil water falls on the Global Meteoric Water Line, that is,

$$\ln(\delta^{17}\text{O}_{\text{soil}} + 1) = \lambda_{\text{GMWL}} \cdot \ln(\delta^{18}\text{O}_{\text{soil}} + 1) + \gamma_{\text{GMWL}}, \quad (14)$$

with  $\lambda_{\text{GMWL}} = 0.528$  and  $\gamma_{\text{GMWL}} = 0.033\text{‰}$  (Luz & Barkan, 2010). The resulting distribution of the  $\Delta^{17}\text{O}_{\text{soil}}$  has a maximum value near the equator and drops to its minimum close to the North Pole; see Figure 5b.

The isotopic signature of leaf water  $\Delta^{17}\text{O}_{\text{leaf}}$  (note that we use the same symbol for the  $\Delta^{17}\text{O}$  signature of  $\text{CO}_2$  that has equilibrated with leaf water, because for our selected reference level  $\lambda_{\text{RL}}$  these two signatures have the same value) is determined from the isotopic signature of soil water  $\Delta^{17}\text{O}_{\text{soil}}$  and the fractionation occurring due to the transpiration of water

$$\Delta^{17}\text{O}_{\text{leaf}} = \Delta^{17}\text{O}_{\text{soil}} + (\lambda_{\text{transp}} - \lambda_{\text{RL}}) \cdot \ln(\alpha_{\text{transp}}), \quad (15)$$

where  $\alpha_{\text{transp}} = 1/0.9917$  (West et al., 2008) is the fractionation factor of transpiration of  $\text{H}_2^{18}\text{O}$  relative to  $\text{H}_2^{16}\text{O}$  and  $\lambda_{\text{transp}}$  is the exponent relating fractionation of  $\text{H}_2^{17}\text{O}$  to transpiration of  $\text{H}_2^{18}\text{O}$

$$\lambda_{\text{transp}} = 0.522 - 0.008 \cdot h, \text{ for } 0.3 \leq h \leq 1, \quad (16)$$

where  $h$  is the relative humidity as was demonstrated by Landais et al. (2006). The resulting spatial distribution and temporal variation of  $\Delta^{17}\text{O}_{\text{leaf}}$  is shown in Figure 5, where we used relative humidity data from ERA-Interim. The isotopic signature  $\Delta^{17}\text{O}_{\text{leaf}}$  attains its maximum in the African Sahara, where relative humidity is low, and has low values in the arctic region. The leaf signature for the northern and southern extratropical regions (NET and SET) exhibits a seasonal cycle of opposite phase with a peak-to-peak amplitude of  $\sim 20$  per meg. The  $\Delta^{17}\text{O}_{\text{leaf}}$  in the tropical region has hardly any seasonality.

To test the effect of the soil water signature  $\Delta^{17}\text{O}_{\text{soil}}$  and the leaf water signature  $\Delta^{17}\text{O}_{\text{leaf}}$  on  $\Delta^{17}\text{O}$  in  $\text{CO}_2$ , we performed simulations with a spatially distributed  $\Delta^{17}\text{O}_{\text{soil}}$  and temporally and spatially distributed  $\Delta^{17}\text{O}_{\text{leaf}}$  (BASE in Table 2) as well as a simulation with a constant soil water signature of  $-5$  per meg (SOIL\_CONST) and a simulation with a constant relative humidity of  $0.8$ , which can be converted using equation (16) to  $\lambda_{\text{transp}} = 0.5156$  (LEAF\_CONST). The results of these simulations are given in section 3.1.3.

### 2.3.2. Respiration and Soil Invasion

The  $\text{CO}_2$  respiration flux is calculated in SiBCASA from multiple above and below ground carbon pools with different turnover rates, depending on temperature and moisture (Schaefer et al., 2008). The calculated respiration flux from SiBCASA is aggregated over a period of 1 month for each  $1^\circ \times 1^\circ$  grid cell. From the monthly respiration fluxes and the ERA-Interim 2-m temperature, the coefficient  $R_0$  is determined (see equation (17) for its definition) and stored in a file. In our TM5 model, the  $\text{CO}_2$  respiration flux depends on temperature (and thus also on time) according to the following  $Q_{10}$  relation (Potter et al., 1993)

$$F_{\text{resp}} = R_0 \cdot Q_{10}^{\frac{T - T_{\text{ref}}}{10}}, \quad (17)$$

with  $Q_{10} = 1.5$  and  $T_{\text{ref}} = 273.5$  K. For  $T$  we used the 2-m temperature from ERA-Interim, which has a spatial resolution of  $1^\circ \times 1^\circ$  and a 3-hourly time resolution, which allows us to simulate a diurnal cycle in the respiration flux. The coefficient  $R_0$  is read from the SiBCASA output file and assures that the aggregated monthly respiration flux calculated according to equation (17) agrees with the monthly respiration flux for each cell from SiBCASA. The global respiration flux that we determine with SiBCASA for 2011 is 129 PgC/year (total respiration, including autotrophic leaf respiration).

The isotopic signature of respired  $\text{CO}_2$  (excluding the autotrophic leaf respired component, calculated similar to the net assimilation flux as described in section 2.3.1) is determined by equilibration with soil water, followed by kinetic fractionation due to diffusion through the soil column into the atmosphere

$$\Delta^{17}\text{O}_{\text{resp}} = \Delta^{17}\text{O}_{\text{soil}} + (\lambda_{\text{kinetic}} - \lambda_{\text{RL}}) \cdot \ln(\alpha_{\text{soil}}), \quad (18)$$

where  $\alpha_{\text{soil}} = 0.9928$  is the kinetic fractionation factor of  $\text{C}^{18}\text{OO}$  relative to  $\text{CO}_2$  for diffusion out of the soil column into the atmosphere (Miller et al., 1999).

The reported magnitudes of the global soil invasion flux cover a wide range: from 30 PgC/year (Stern et al., 2001) to 450 PgC/year (Wingate et al., 2009). The high soil invasion flux estimate is explained by the presence of the enzyme carbonic anhydrase in soils (Wingate et al., 2009). Similar to  $\text{CO}_2$ , soil invasion fluxes of carbonyl sulfide (COS) are also affected by carbonic anhydrase (Ogée et al., 2016). The soil uptake of COS has been modeled by Launois et al. (2015) assuming that COS uptake scales linearly with  $v_{\text{dep}}$ , the deposition velocity of molecular hydrogen to soils (based on the assumption that both processes are affected by similar soil microorganisms).

In this study, the global magnitude of the soil invasion flux is set to 30 PgC/year by default (normalized for years 2012–2013) but can be changed to any user-specified value. Also, the spatial distribution of the soil invasion flux can be scaled with the biosphere  $\text{CO}_2$  respiration flux (i.e.,  $F_{\text{SIA}} \propto F_{\text{resp}}$ ) or alternatively the hydrogen deposition velocity (i.e.,  $F_{\text{SIA}} \propto v_{\text{dep}}$ ). See Table 1 for an overview of the available model settings for the soil invasion flux. To test the sensitivity of the  $\Delta^{17}\text{O}$  signature of atmospheric  $\text{CO}_2$  on the magnitude and spatial distribution of the soil invasion flux, we performed four additional simulations (RESP\_240, RESP\_450, HYD\_240, and HYD\_450 that are summarized in Table 2), for which the results are discussed in section 3.1.3.

The isotopic signature of  $\text{CO}_2$  that diffuses into soils (“ASI”) is determined from the local atmospheric  $\Delta^{17}\text{O}$  as predicted by our model. The  $\Delta^{17}\text{O}$  signature of  $\text{CO}_2$  released from the soil (“SIA”) is set equal to the signature of soil water  $\Delta^{17}\text{O}_{\text{soil}}$  described in section 2.3.1. Isotopic fractionation is not taken into account for the soil invasion fluxes, since the ingoing and outgoing fluxes have equal magnitude in our model (i.e.,  $F_{\text{SIA}} = -F_{\text{ASI}}$ ), and therefore, the kinetic fractionation effect on the atmospheric  $\Delta^{17}\text{O}$  budget cancels out.



### 2.3.3. Ocean Exchange

The exchange of CO<sub>2</sub> between the atmosphere and the ocean is based on the relationship between wind speed and gas exchange over the ocean as reported by Wanninkhof (1992). The gas transfer coefficient  $k$ , in centimeter per hour, is calculated from

$$k = 0.31 \cdot u^2 \cdot \left[ \frac{Sc}{660} \right]^{-0.5}, \quad (19)$$

where  $u$  is the wind speed in meter per second and  $Sc$  is the dimensionless Schmidt number. Note that the coefficient 0.31 in equation (19) is not dimensionless. Now, the two-way CO<sub>2</sub> exchange fluxes can be determined from

$$F_{AO} = k \cdot s \cdot p_{CO_2}, \quad F_{OA} = k \cdot s \cdot (p_{CO_2} + \Delta p_{CO_2}), \quad (20)$$

where  $s$  is the solubility of CO<sub>2</sub> in ocean water expressed in mol per cubic meter per atmosphere,  $p_{CO_2}$  is the partial pressure of CO<sub>2</sub> in the atmosphere in unit  $\mu$  atmosphere ( $\approx 0.1$  Pa), and  $\Delta p_{CO_2}$  is the CO<sub>2</sub> partial pressure difference between the ocean and the atmosphere in unit  $\mu$  atmosphere. When we express  $k$  in meter per second, the CO<sub>2</sub> fluxes have units of mol per squared meter per second. For cells that are covered with sea ice, the exchange fluxes are set to zero. The sea ice cover and wind speed data are taken from the ERA-Interim data set (Dee et al., 2011), with a time resolution of 3 hr and a horizontal resolution of  $1^\circ \times 1^\circ$ . Data for solubility, CO<sub>2</sub> partial pressure difference, and the Schmidt number are taken from Jacobson et al. (2007) with a horizontal resolution of  $5^\circ \times 4^\circ$  and a temporal resolution of 1 month.

The isotopic signature of ocean water is taken as  $\Delta^{17}O_{\text{ocean}} = -0.005\text{‰}$  (Luz & Barkan, 2010). Note that equilibration between CO<sub>2</sub> and H<sub>2</sub>O does not result in a fractionation of our  $\Delta^{17}O$  signal, because we have taken the CO<sub>2</sub>-H<sub>2</sub>O equilibration constant as our reference line (i.e.,  $\lambda_{RL} = \lambda_{CO_2-H_2O}$ ). We have neglected the kinetic fractionation effect for diffusion across the ocean-atmosphere interface, since the associated fractionation factor for C<sup>18</sup>OO relative to CO<sub>2</sub> is close to 1 ( $\alpha_{\text{ocean}} \approx 0.9992$  according to Vogel et al., 1970) and the gross ocean fluxes largely cancel out (with a difference of  $\sim 3$  PgC/year on the global scale; see Figure 1).

In our model, the ocean sink for the CO<sub>2</sub> and C<sup>17</sup>OO tracers can be determined from predefined constant CO<sub>2</sub> and C<sup>17</sup>OO concentrations or dynamically coupled to the local concentrations of CO<sub>2</sub> and C<sup>17</sup>OO above the ocean surface that the model calculates each time step (see Table 1 for an overview of the available model settings). For the results that we include in this paper, we always used the dynamic coupling between the ocean sink and the local atmospheric concentration.

### 2.3.4. Fossil Fuel Combustion and Biomass Burning

The CO<sub>2</sub> fluxes from fossil combustion in our model are based on the Emissions Database for Global Atmospheric Research (EDGAR) version 4.2 from the Joint Research Centre of the European Union. The temporal resolution of this data set was improved by coupling to country and sector-specific time profiles by the Institute for Energy Economics and the Rational Use of Energy from the University of Stuttgart. For our model we use the CO<sub>2</sub> fluxes with a monthly time resolution and a horizontal resolution of  $1^\circ \times 1^\circ$ . We assign a signature of  $\Delta^{17}O_{ff} = -0.386\text{‰}$  to the CO<sub>2</sub> that is released by fossil fuel combustion, which is largely determined by the  $\Delta^{17}O$  signature of ambient O<sub>2</sub> (Horváth et al., 2012). Laskar et al. (2016) reconstructed the same  $\Delta^{17}O$  signature for CO<sub>2</sub> from car exhausts measured in a tunnel.

The CO<sub>2</sub> released to the atmosphere by biomass burning is taken from the Global Fire Emissions Database version 4 (GFED4; Giglio et al., 2013). This data set is comprised by combining remotely sensed burned areas with modeled carbon pools from SiBCASA (van der Werf et al., 2010; van der Velde et al., 2014). The SiBCASA biomass burning emissions are available with a monthly time resolution and a spatial resolution of  $1^\circ \times 1^\circ$ . The isotopic signature of CO<sub>2</sub> released by biomass burning is determined by the isotopic signature of ambient O<sub>2</sub> and the wood intrinsic oxygen, resulting in an average signature of  $\Delta^{17}O_{bb} = -0.230\text{‰}$  for released CO<sub>2</sub> (Horváth et al., 2012).

## 2.4. Tropospheric Source of $\Delta^{17}O$ in CO<sub>2</sub>

### 2.4.1. Tropospheric CO and $\Delta^{17}O(\text{CO})$ Budget

Most of the atmospheric CO<sub>2</sub> originates from the Earth surface, where it is released directly in the form of CO<sub>2</sub> through one of the processes as described in section 2.3. In addition, CO<sub>2</sub> can be produced in the atmosphere through oxidation of atmospheric CO by the hydroxyl radical OH,



In this section we describe observed spatiotemporal patterns in  $\Delta^{17}\text{O}(\text{CO})$ , the processes driving  $\Delta^{17}\text{O}(\text{CO})$  and the implications for the production of  $\text{CO}_2$  isotopologues. Subsequently, we describe in section 2.4.2 how the production of  $\text{CO}_2$  isotopologues from CO oxidation is implemented in our 3-D atmospheric transport model.

Measurements have revealed a large positive  $\Delta^{17}\text{O}$  signature in atmospheric CO varying with season and location (measured at the per mil scale, similar to stratospheric  $\text{CO}_2$  shown in Figure 2). Huff and Thiemens (1998) report that  $\Delta^{17}\text{O}(\text{CO})$  increases from a minimum of  $\sim 0.3\text{‰}$  during winter to a maximum of  $\sim 2.7\text{‰}$  during summer months in San Diego, California. Röckmann et al. (2002) measured a  $\Delta^{17}\text{O}(\text{CO})$  winter minimum of  $\sim 2\text{‰}$  and summer maximum of  $\sim 8\text{‰}$  at high northern latitude stations in Alert, Canada, and Spitsbergen, Norway. At the tropical station Izaña, Tenerife, the seasonal cycle of  $\Delta^{17}\text{O}(\text{CO})$  is much lower ( $\sim 1\text{‰}$ ) but the annual average value is rather similar at about  $5\text{‰}$  (Röckmann et al., 1998a).

The most important source of the large  $\Delta^{17}\text{O}$  signature of CO is the oxidation of CO by OH (Röckmann et al., 1998a), which is not a mass-dependent process (the rate coefficients for oxidation of  $\text{C}^{16}\text{O}$  and  $\text{C}^{17}\text{O}$  are approximately equal, whereas the rate coefficient for  $\text{C}^{18}\text{O}$  is substantially higher than for  $\text{C}^{17}\text{O}$ ). This explains the observed seasonal cycle of  $\Delta^{17}\text{O}(\text{CO})$ , since OH levels are higher during the summer months than during winter months, which is more pronounced at higher latitudes. Besides this main oxidation sink with a global magnitude of  $\sim 1$  PgC/year (Holloway et al., 2000), CO is also taken up by soils at a global rate of  $0.05\text{--}0.1$  PgC/year (Sanhueza et al., 1998) which is a mass-dependent process and thus not affecting  $\Delta^{17}\text{O}(\text{CO})$ .

Another contribution to the positive  $\Delta^{17}\text{O}$  in CO is the ozonolysis of nonmethane hydrocarbons (Röckmann et al., 1998b), but its effect on the  $\Delta^{17}\text{O}(\text{CO})$  budget is less strong than the effect of the oxidation reaction. The main sources of CO (i.e., fossil fuel combustion, biomass burning and oxidation of atmospheric hydrocarbons) are considered to have a negligible contribution to the  $\Delta^{17}\text{O}(\text{CO})$  budget (Brenninkmeijer et al., 1999).

The sources and sinks of CO and their isotopic composition are uncertain and characterized by strong spatial and temporal variability but allow us to describe the following implications for the production of  $\Delta^{17}\text{O}$  in  $\text{CO}_2$ . As the OH levels increase after winter, the mass-independent OH sink in equation (21) results in the production of  $\text{CO}_2$  with a negative  $\Delta^{17}\text{O}$  signature and the simultaneous increase in  $\Delta^{17}\text{O}$  of the remaining CO. Due to the increasing enrichment of the substrate  $\text{C}^{17}\text{O}$  and depletion of the substrate  $\text{C}^{18}\text{O}$ , the  $\Delta^{17}\text{O}$  isoflux from CO to  $\text{CO}_2$  will increase (i.e., become more positive or less negative) during the summer months. Since the sources of CO are largely mass dependent (i.e., with  $\Delta^{17}\text{O}(\text{CO}) \approx 0$ ) and nearly all CO is removed through OH oxidation, we infer from mass conservation that the annual mean contribution of CO oxidation to the global budget of  $\Delta^{17}\text{O}$  in  $\text{CO}_2$  is minor (as will be confirmed in section 3.1.3.)

#### 2.4.2. Production of $\text{CO}_2$ Isotopologues

To simulate the production of  $\Delta^{17}\text{O}$  in  $\text{CO}_2$  from CO oxidation, we use climatological fields for  $\text{C}^{16}\text{O}$ ,  $\text{C}^{17}\text{O}$  and  $\text{C}^{18}\text{O}$  from Gromov (2013) with a global mean  $\Delta^{17}\text{O}(\text{CO})$  signature of  $5.0\text{‰}$  and climatological OH fields from Spivakovsky et al. (2000). The OH fields are available for each month on a native TM5 resolution of  $1^\circ \times 1^\circ$  horizontally and 60 vertical sigma-pressure levels. The climatological CO isotopologue fields are provided with a 5-day time resolution on a T42 spectral resolution and a vertical grid of 19 hybrid sigma-pressure levels and are regridded to match the temporal and spatial resolution of the OH fields.

We use a pressure-dependent relation for the rate of oxidation of CO from DeMore et al. (1997)

$$k_{\text{CO}+\text{OH}} = 1.5 \cdot 10^{-13} \cdot (1 + 0.6 \cdot p), \quad (22)$$

where  $p$  is the atmospheric pressure in the unit atmosphere and the unit of the rate coefficient  $k_{\text{CO}+\text{OH}}$  is cubic centimeter per molecule per second. In our model this rate coefficient is based on climatological pressure fields derived from the orography of the Earth surface. The rate coefficients for the oxidation of the isotopologues  $\text{C}^{17}\text{O}$  and  $\text{C}^{18}\text{O}$  are determined with respect to the overall rate coefficient from

$$\epsilon_n = k_{\text{CO}+\text{OH}}/k_{\text{C}^n\text{O}+\text{OH}} - 1, \quad (23)$$

for  $n = 17$  or  $18$ . The enrichment  $\epsilon_n$  was measured in a controlled lab environment by Röckmann et al. (1998a) as  $\epsilon_{17} = -0.21 \pm 1.30\text{‰}$  and  $\epsilon_{18} = -9.29 \pm 1.52\text{‰}$  (for atmospheric pressure, according to Table 3.6 in Gromov, 2013). In a different lab study by Feilberg et al. (2002, 2005) enrichments of  $\epsilon_{17} = 0 \pm 4\text{‰}$

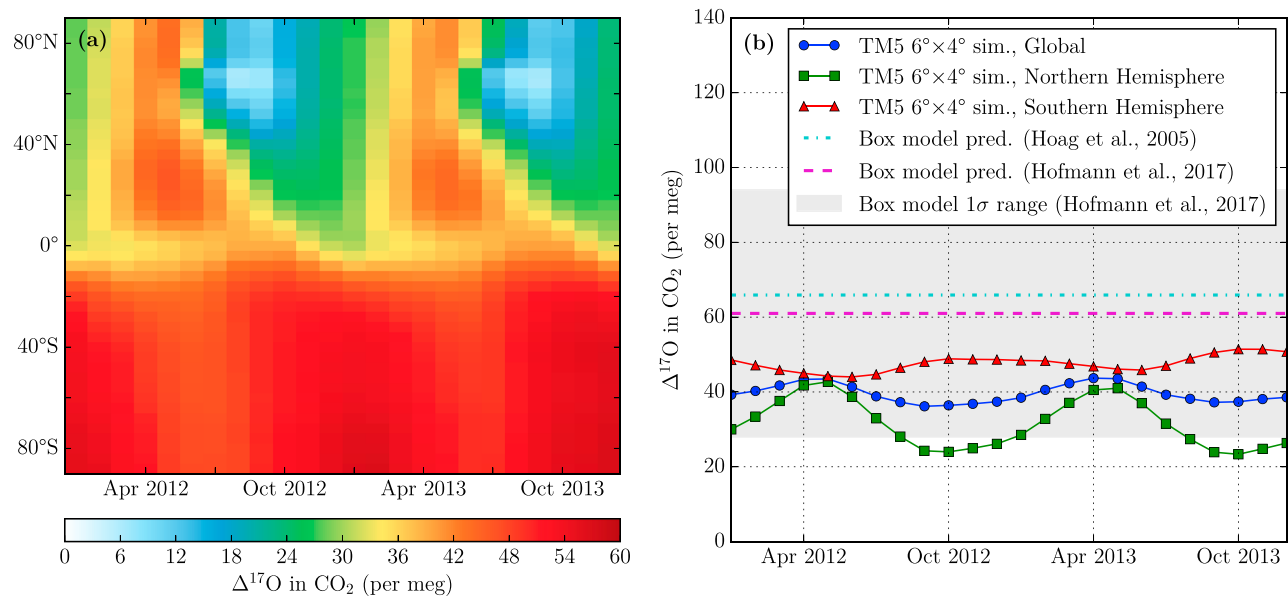


**Figure 6.** Monthly average of simulated  $\Delta^{17}\text{O}$  in  $\text{CO}_2$  for the lowest 500 m of the atmosphere using the TM5 model with base settings and a  $6^\circ \times 4^\circ$  horizontal resolution and 25 vertical levels. (a) Hovmöller diagram of  $\Delta^{17}\text{O}$  in  $\text{CO}_2$ . (b) Time series of  $\Delta^{17}\text{O}$  in  $\text{CO}_2$  for TM5 integrated over NH, SH, and global domain, compared with predictions from box models by Hoag et al. (2005) and Hofmann et al. (2017).

and  $\epsilon_{18} = -15 \pm 5\text{‰}$  were found. To test the consequences of applying the different rate coefficients, we have performed simulations for both lab results (simulations CO\_ROCK and CO\_FEIL, as summarized in Table 2).

The oxygen in atmospheric OH likely does not have an anomalous  $\Delta^{17}\text{O}$  signature, since it equilibrates rapidly with atmospheric water vapor (Dubey et al., 1997; Lyons, 2001) and the  $\Delta^{17}\text{O}$  signature of water vapor is negligible compared to that of CO (Uemura et al., 2010). To calculate the production of  $\text{CO}_2$  isotopologues in our model, we assumed that  $\Delta^{17}\text{O}(\text{OH}) = 0\text{‰}$ , such that the temporal and spatial variation in the  $\text{CO}_2$  production fields is determined fully by that of the CO isotopologues, the OH concentration, and the rate coefficients in equations (22) and (23). To prevent interference with the stratospheric model described in section 2.2, we only apply the chemical production of  $\Delta^{17}\text{O}$  between the Earth surface and the 100-hPa level.

From the derived  $\text{C}^{16}\text{OO}$ ,  $\text{C}^{17}\text{OO}$ , and  $\text{C}^{18}\text{OO}$  production fields, we calculated the associated  $\Delta^{17}\text{O}$  “flux” field. Subsequently, we scaled the  $\text{C}^{18}\text{OO}$  fluxes such that the  $\delta^{18}\text{O}$  fields for produced  $\text{CO}_2$  equal our assumed fixed value of 41.5‰ (see section 2.1). Finally, we scaled the  $\text{C}^{17}\text{OO}$  flux fields to reobtain the  $\Delta^{17}\text{O}$  flux field. As mentioned in section 2.1, the motivation for using a fixed  $\delta^{18}\text{O}$  for atmospheric  $\text{CO}_2$  is that this considerably simplifies the coupling with the hydrological cycle. This method implies that the simulated  $\Delta^{17}\text{O}$  signature is fully carried by the  $\text{C}^{17}\text{OO}$  tracer in our atmospheric transport model.

Note that the contribution of mass-independent  $\text{CO}_2$  through oxidation of atmospheric CO was not considered in the previous box models from Hoag et al. (2005) and Hofmann et al. (2017). Likewise, oxidation of CO is not included in our model runs with base settings (BASE), as summarized in Table 1. The resulting  $\Delta^{17}\text{O}$  in atmospheric  $\text{CO}_2$  for the simulations CO\_ROCK and CO\_FEIL (see Table 2) is presented and discussed in section 3.1.3.

### 3. Results

#### 3.1. Global Model Simulations

##### 3.1.1. $\Delta^{17}\text{O}$ in Tropospheric $\text{CO}_2$ for Base Model

In this section we show the results from the TM5 simulation with the base settings as summarized in Table 1 at a horizontal resolution of  $6^\circ \times 4^\circ$  and with 25 vertical levels. We started a simulation with an initial  $\text{CO}_2$  distribution from data assimilation system CarbonTracker (Peters et al., 2007, 2010; van der Laan-Luijkx et al., 2017) and with  $\Delta^{17}\text{O} = 0$  for each cell. After running the model for  $\sim 10$  years, we obtained a steady state (no further increase in the mean annual  $\Delta^{17}\text{O}$  signature) for the years 2012 and 2013 for which we show the results. We provide insight into the temporal and spatial patterns of modeled  $\Delta^{17}\text{O}$  in  $\text{CO}_2$  for the

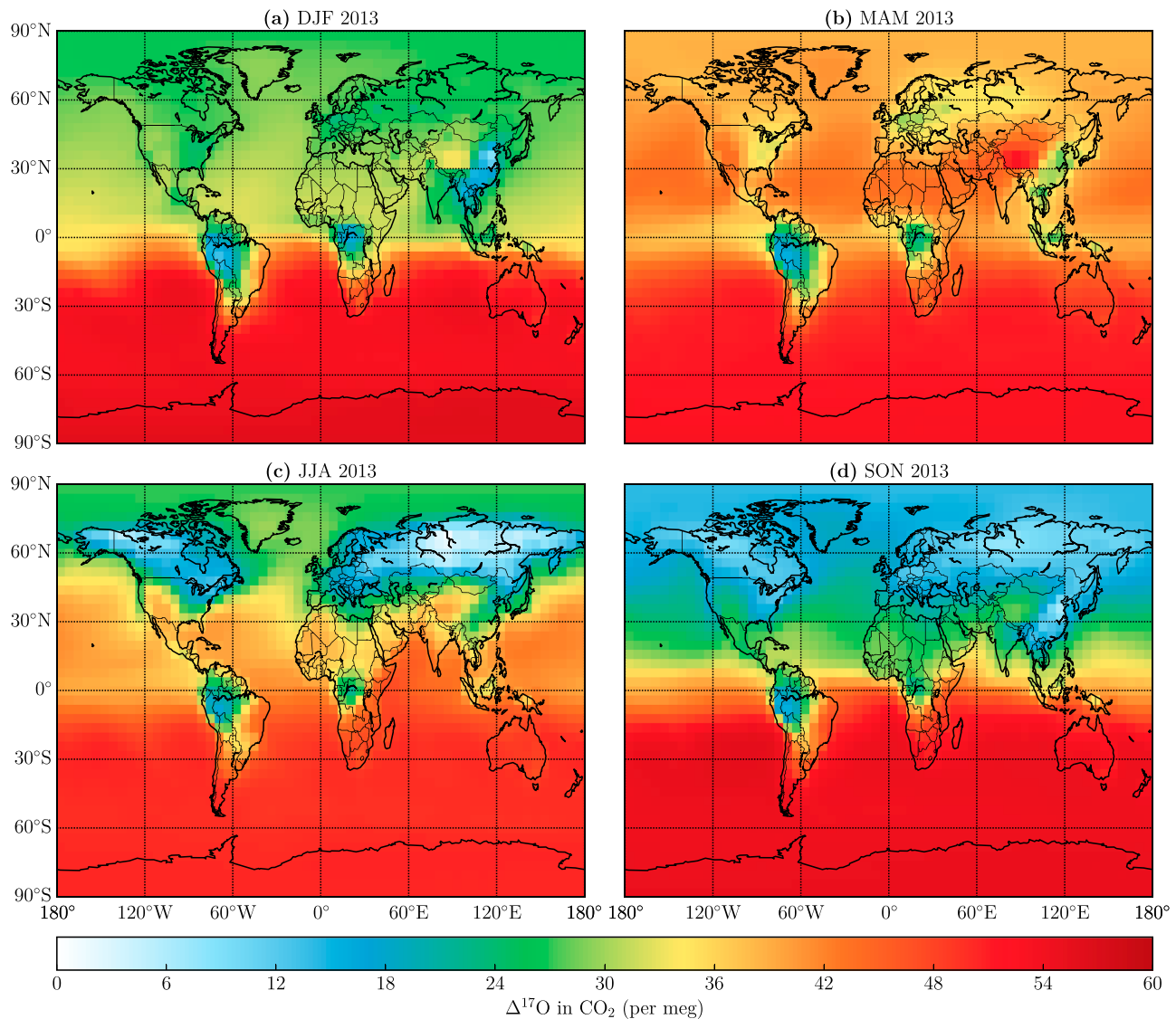


**Figure 7.** Seasonal average distributions of simulated  $\Delta^{17}\text{O}$  in  $\text{CO}_2$  for lowest 500 m of atmosphere from the TM5 model with base settings using a  $6^\circ \times 4^\circ$  horizontal resolution and 25 vertical levels. (a) Seasonal average for December, January, and February (DJF) 2013. (b) Seasonal average for March, April, and May (MAM) 2013. (c) Seasonal average for June, July, and August (JJA) 2013. (d) Seasonal average for September, October, and November (SON) 2013.

lowest  $\sim 500$  m of the atmosphere (lowest four model levels). The  $\text{CO}_2$  mass fluxes and corresponding  $\Delta^{17}\text{O}$  isofluxes between the different reservoirs are discussed in section 3.1.2.

In Figure 6, we show the temporal variation of monthly average  $\Delta^{17}\text{O}$  in  $\text{CO}_2$ . The Hovmöller diagram in Figure 6a shows that the Northern Hemisphere experiences the largest seasonal variation and that the decrease in  $\Delta^{17}\text{O}$  occurs during the summer months for both hemispheres. Figure 6b shows the temporal variation of  $\Delta^{17}\text{O}$  in  $\text{CO}_2$  integrated over both hemispheres and for the global domain compared to box model predictions from Hoag et al. (2005) and Hofmann et al. (2017). Our 3-D model predicts an average  $\Delta^{17}\text{O}$  signature of 39.6 per meg for  $\text{CO}_2$  in the lowest 500 m of the atmosphere, which is roughly 20 per meg lower than the prediction from the box model by Hofmann et al. (2017). This is an expected result since the exchange of  $\text{CO}_2$  with the biosphere, which represents the main sink of  $\Delta^{17}\text{O}$ , is higher in our model than for the box models. For the NH and SH we predict a mean  $\Delta^{17}\text{O}$  signature of 31.6 and 47.6 per meg and a seasonal cycle with a peak-to-peak amplitude of 17.7 and 5.1 per meg, respectively. The spatial and temporal patterns in simulated  $\Delta^{17}\text{O}$  confirm the potential of  $\Delta^{17}\text{O}$  as a tracer of GPP.

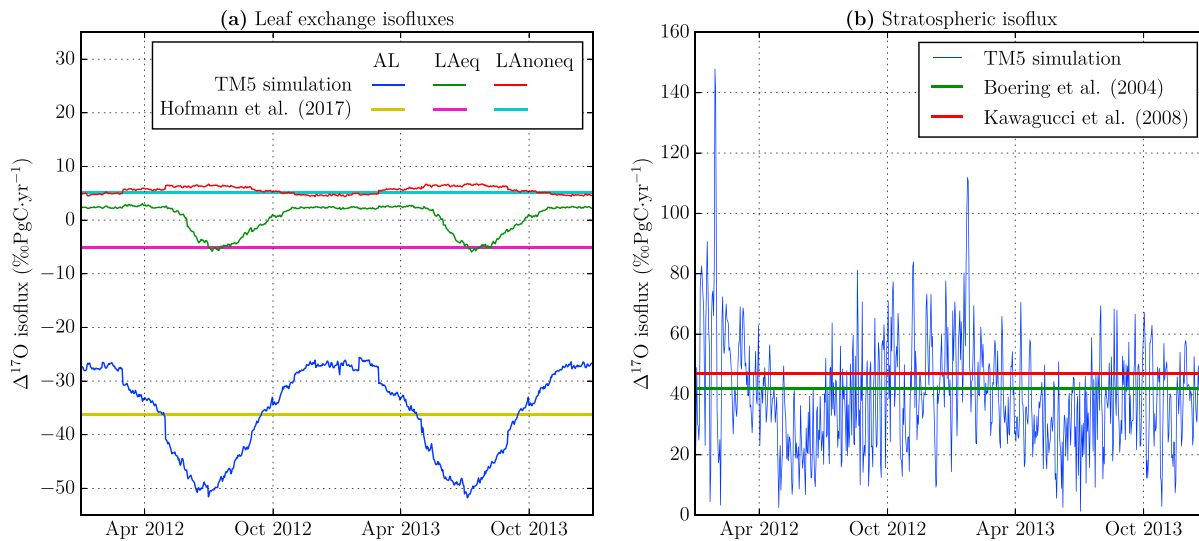


**Figure 8.** Daily time series of main  $\Delta^{17}\text{O}$  isofluxes for TM5 simulation using base settings with  $6^\circ \times 4^\circ$  horizontal resolution and 25 vertical levels compared with independent global estimates. (a) Leaf exchange isofluxes from TM5 compared with predictions from the box model from Hofmann et al. (2017). (b) Net stratosphere-troposphere  $\Delta^{17}\text{O}$  isoflux simulated with TM5 model compared with global estimates from Boering et al. (2004) and Kawagucci et al. (2008) based on observed  $\text{N}_2\text{O}$ – $\Delta^{17}\text{O}$  correlation and the stratospheric  $\text{N}_2\text{O}$  loss rate.

The spatial distribution of  $\Delta^{17}\text{O}$  for the different seasons of 2013 is shown in Figure 7. Besides the North-South gradient that was already visible in Figure 6, we can see that the  $\Delta^{17}\text{O}$  signature over oceans exceeds the  $\Delta^{17}\text{O}$  above land, which can be explained by the strong effect of the biosphere on atmospheric  $\Delta^{17}\text{O}$ . In addition, the tropical regions in South America and Africa have low  $\Delta^{17}\text{O}$  values during the entire year, with large zonal gradients, especially during December, January, and February and September, October, and November. Although the exchange of  $\text{CO}_2$  between the biosphere and atmosphere is highest for the tropical regions, the lowest  $\Delta^{17}\text{O}$  occurs in the NET. This is a direct consequence of the low  $\Delta^{17}\text{O}$  signatures of soil water and leaf water (see Figure 5c) in the NET compared to the tropics. Note also that fossil fuel combustion can have a strong effect on the local  $\Delta^{17}\text{O}$  signal, which explains the low  $\Delta^{17}\text{O}$  in  $\text{CO}_2$  simulated over parts of China.

### 3.1.2. $\text{CO}_2$ Mass Fluxes and $\Delta^{17}\text{O}$ Isofluxes for Base Model

To better understand the  $\Delta^{17}\text{O}$  budget, we analyzed the magnitudes and spatiotemporal variations of the simulated  $\text{CO}_2$  mass fluxes and  $\Delta^{17}\text{O}$  isofluxes. The definition of the  $\Delta^{17}\text{O}$  isoflux is

$$IF_{ij} = F_{ij} \cdot (\Delta^{17}\text{O}_i - \Delta^{17}\text{O}_{\text{trop}}), \quad (24)$$

where  $IF_{ij}$  and  $F_{ij}$  are, respectively, the  $\Delta^{17}\text{O}$  isoflux and  $\text{CO}_2$  mass flux from reservoir  $i$  to reservoir  $j$ . Furthermore,  $\Delta^{17}\text{O}_{\text{trop}}$  and  $\Delta^{17}\text{O}_i$  are the signatures for the troposphere and for the source reservoir (which can also be the troposphere, e.g., for the isoflux from the atmosphere to the ocean  $IF_{\text{AO}}$ ). In this study we have used a reference level of  $\Delta^{17}\text{O}_{\text{trop}} = 40$  per meg, which is representative for the lowest  $\sim 500$  m of the atmosphere as described in section 3.1.1. The globally averaged yearly averaged  $\text{CO}_2$  mass fluxes and  $\Delta^{17}\text{O}$  isofluxes simulated by our TM5 model and the fluxes from the box models by Hofmann et al. (2017) and Hoag et al. (2005) are summarized in Table S2 of the supporting information.

In Figure 8 we show the global time series of the main biospheric and stratospheric  $\Delta^{17}\text{O}$  isofluxes from the model simulation with base settings for the years 2012–2013. For the global biospheric  $\Delta^{17}\text{O}$  isofluxes shown in Figure 8a, the atmosphere-leaf isoflux  $IF_{\text{AL}}$  has the largest seasonal variation with a peak-to-peak amplitude of  $\sim 25\%$   $\text{PgC}/\text{year}$ .  $IF_{\text{AL}}$  attains its peak (i.e., the most negative value) during the summer months in the Northern Hemisphere, similar to the seasonality in global carbon uptake by vegetation. The global equilibrated leaf-atmosphere isoflux  $IF_{\text{LAeq}}$  has a seasonal cycle with peak-to-peak amplitude of  $\sim 10\%$   $\text{PgC}/\text{year}$  and is changing sign during the course of the year. The sign change in  $IF_{\text{LAeq}}$  is related to the change in the isotopic signature of leaf water (see section 2.3.1) and the selected reference level  $\Delta^{17}\text{O}_{\text{trop}}$ . Finally, we see that global mean nonequilibrated leaf-atmosphere isoflux  $IF_{\text{LAnoneq}}$  is nearly constant during the year. Note



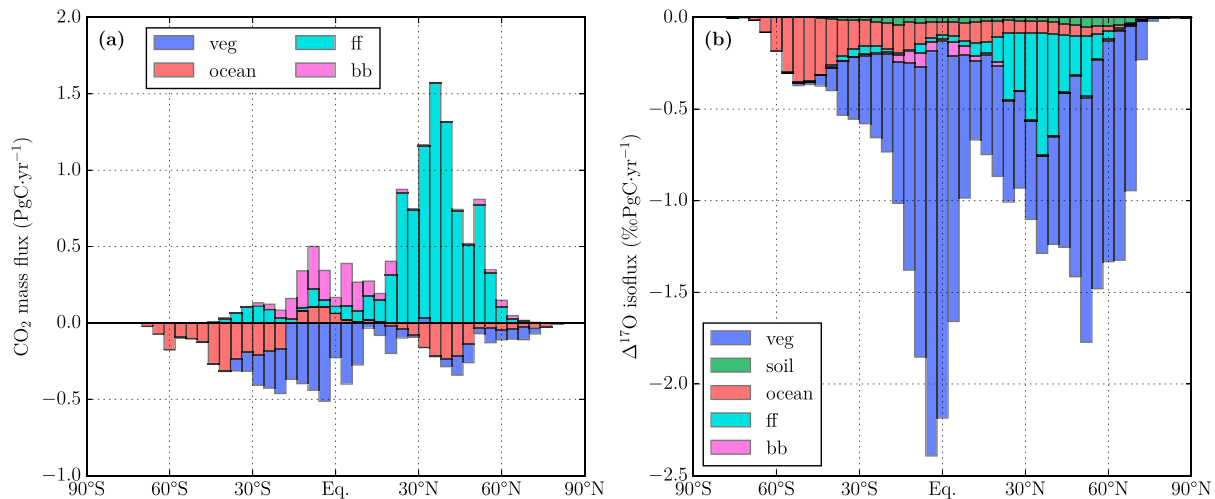


**Figure 9.** Net CO<sub>2</sub> mass fluxes (a) and net Δ<sup>17</sup>O isofluxes (b) as function of latitude resulting from vegetation exchange (“veg”), soil invasion, ocean exchange, fossil fuel combustion (“ff”), and biomass burning (“bb”) for TM5 simulation with base settings, 6° × 4° horizontal resolution, and 25 vertical levels.

that for all biospheric fluxes shown in Figure 8a the average value (and hence also the occurrence of sign changes for  $IF_{\text{LAeq}}$ ) is sensitive to the reference level  $\Delta^{17}\text{O}_{\text{trop}}$ .

The global net stratospheric Δ<sup>17</sup>O isoflux in Figure 8b has a mean value of ~40‰ PgC/year, which agrees well with the estimates from Boering et al. (2004) and Kawagucci et al. (2008) that were derived from the observed N<sub>2</sub>O–Δ<sup>17</sup>O correlation and the estimated stratospheric N<sub>2</sub>O loss rate. Also, our global mean Δ<sup>17</sup>O stratospheric isoflux is close to the simulated flux by Liang et al. (2008). Our simulated stratospheric Δ<sup>17</sup>O isoflux has a seasonal cycle with a peak-to-peak amplitude of ~40‰ PgC/year. On top of this, a relatively large day-to-day variability is associated with the stratospheric Δ<sup>17</sup>O isoflux. The average value of the stratospheric isoflux is not sensitive (compared to biospheric isofluxes) to small changes in the reference level, since  $\Delta^{17}\text{O}_{\text{strat}} \gg \Delta^{17}\text{O}_{\text{trop}}$  whereas  $\Delta^{17}\text{O}_{\text{leaf}} \approx \Delta^{17}\text{O}_{\text{trop}}$ . During the Northern Hemispheric winter months, the global stratospheric influx of Δ<sup>17</sup>O is relatively high, while at the same time the biospheric sink of Δ<sup>17</sup>O is relatively weak, resulting in an increase of Δ<sup>17</sup>O in atmospheric CO<sub>2</sub> on the global scale (which is visible in Figure 6). An overview of the temporal variation of all global CO<sub>2</sub> mass fluxes and Δ<sup>17</sup>O isofluxes during the years 2012–2013 is given in Figures S2 and S3 of the supporting information.

The latitudinal distribution of the annual mean net CO<sub>2</sub> mass fluxes and Δ<sup>17</sup>O isofluxes for 2012–2013 is shown in Figure 9 for different surface processes. Figure 9a clearly shows the dominance of fossil fuel combustion (“ff”) in the CO<sub>2</sub> budget. In the warm tropics, the ocean is a source of CO<sub>2</sub> to the atmosphere ( $F_{\text{OA}} > F_{\text{AO}}$ ), whereas the ocean is a net sink of CO<sub>2</sub> in the extratropics. Across all latitudes, vegetation exchange and biomass burning act as a net sink and source, respectively, and both processes peak in the tropical region. Soil invasion has no net contribution to the CO<sub>2</sub> budget, since we assume that the uptake is equal to the release for each grid cell. The Δ<sup>17</sup>O isofluxes in Figure 9b are negative for all latitudinal bands for each surface process. The Δ<sup>17</sup>O isofluxes are dominated by the vegetation fluxes, although the contribution of fossil fuel combustion is significant in the Northern Hemisphere. Soil invasion Δ<sup>17</sup>O isofluxes are relatively small, for this simulation with base settings. More details for the contribution of different processes (e.g., the ingoing and outgoing leaf fluxes) as a function of latitude are presented in Figures S4 and S5 of the supporting information.

### 3.1.3. Model Sensitivity Analysis

Here we discuss the results of a sensitivity analysis for Δ<sup>17</sup>O in CO<sub>2</sub>. We have changed input values for the stratospheric N<sub>2</sub>O–Δ<sup>17</sup>O fit coefficients, the soil water and leaf water Δ<sup>17</sup>O signatures, the soil invasion fluxes, and the oxidation of atmospheric CO, as summarized in Table 2. In Table 3 we report the mean value and the peak-to-peak amplitude for Δ<sup>17</sup>O in CO<sub>2</sub> for the lowest 500 m of the atmosphere for a selection of simulations with modified input settings. The peak-to-peak amplitude of global Δ<sup>17</sup>O was determined by fitting a sine function on the monthly values for global Δ<sup>17</sup>O for the years 2012 and 2013.

**Table 3**

Overview of the Mean Value and the Peak-to-Peak Amplitude of the Seasonal Cycle of  $\Delta^{17}\text{O}$  in  $\text{CO}_2$  for the Lowest 500 m of the Atmosphere for Different TM5 Model Simulations with Horizontal Resolution of  $6^\circ \times 4^\circ$  and with 25 Vertical Levels

Simulation	Mean $\Delta^{17}\text{O}$ value (first column; per meg)						
	Peak-to-peak $\Delta^{17}\text{O}$ amplitude (second column, enclosed in parentheses; per meg)						
	Global	NH	SH	Zotino	Mauna Loa	Manaus	South Pole
BASE	39.6 (6.5)	31.6 (17.7)	47.6 (5.1)	19.0 (36.1)	36.2 (19.5)	23.2 (2.9)	52.5 (7.4)
ST_LOWER	19.6 (5.4)	12.6 (14.4)	26.6 (3.9)	1.5 (31.4)	16.3 (15.5)	8.2 (2.9)	30.4 (5.5)
ST_UPPER	59.6 (7.7)	50.6 (21.1)	68.7 (6.3)	36.4 (40.9)	56.1 (23.5)	38.1 (2.9)	74.5 (9.2)
SOIL_CONST	40.5 (4.7)	34.7 (14.3)	46.3 (5.3)	27.8 (23.9)	38.7 (16.8)	18.5 (1.3)	51.1 (7.5)
LEAF_CONST	34.5 (6.7)	26.2 (17.8)	42.8 (4.9)	13.8 (36.1)	30.8 (19.7)	20.0 (2.3)	47.7 (7.1)
RESP_240	32.1 (6.4)	23.5 (17.4)	40.8 (4.9)	9.1 (35.3)	28.3 (19.2)	17.6 (3.0)	45.7 (7.2)
RESP_450	27.6 (6.3)	18.5 (17.1)	36.7 (4.8)	2.7 (34.5)	23.5 (18.9)	14.8 (3.0)	41.7 (7.0)
HYD_240	30.4 (6.6)	21.9 (17.7)	39.0 (4.9)	9.5 (35.6)	26.6 (19.3)	16.4 (3.1)	43.9 (7.1)
HYD_450	25.5 (6.6)	16.6 (17.5)	34.3 (4.7)	4.0 (35.5)	21.4 (19.0)	13.0 (3.1)	39.2 (6.9)
CO_ROCK	40.0 (6.5)	32.0 (17.6)	48.0 (5.1)	19.4 (36.0)	36.6 (19.4)	23.5 (2.9)	52.8 (7.4)
CO_FEIL	37.7 (6.4)	29.8 (17.5)	45.6 (5.1)	17.4 (35.5)	34.2 (19.3)	21.6 (3.1)	50.4 (7.3)

*Note.* The input settings for each simulation are summarized in Table 2. The global and hemispheric results are discussed in section 3.1.3, and the results for Zotino ( $60.80^\circ\text{N}$ ,  $89.35^\circ\text{E}$ ), Mauna Loa ( $19.54^\circ\text{N}$ ,  $155.58^\circ\text{W}$ ), Manaus ( $2.15^\circ\text{S}$ ,  $59.00^\circ\text{W}$ ), and South Pole ( $90^\circ\text{S}$ ) are discussed in section 3.2.2. NH = Northern Hemisphere; SH = Southern Hemisphere.

According to Table 3, the change in the stratospheric  $\text{N}_2\text{O}$ – $\Delta^{17}\text{O}$  fit coefficients results in a change of roughly +20 and –20 per meg for the 95% upper (ST\_UPPER) and lower limit (ST\_LOWER) fits, respectively (see Figure 2b for the slope and offset of the fits) relative to the base model run (BASE). Clearly, the selected stratospheric fit is a key parameter for the resulting  $\Delta^{17}\text{O}$  in tropospheric  $\text{CO}_2$ . Also, we see that the SH–NH difference and the amplitude of global  $\Delta^{17}\text{O}$  increases when using the 95% upper limit confidence interval fit. As expected, the changes in these characteristics of the  $\Delta^{17}\text{O}$  distribution are reversed when using the 95% lower limit confidence interval fit. On annual basis, the effect of changing the stratospheric fit coefficients is smallest for the tropical forests in the Amazon and in Central Africa, as shown in Figure S6 of the supporting information, which is caused by the rapid exchange between the atmosphere and biosphere in these regions.

In the base model run, we use a spatial distribution for the soil water signature  $\Delta^{17}\text{O}_{\text{soil}}$  and spatial and temporal variation in the leaf water signature  $\Delta^{17}\text{O}_{\text{leaf}}$  based on the local relative humidity, according to equations (15) and (16). We performed TM5 simulations with a constant soil water signature  $\Delta^{17}\text{O}_{\text{soil}} = -5$  per meg (SOIL\_CONST) and with a constant transpiration exponent  $\lambda_{\text{transp}} = 0.5156$  (LEAF\_CONST; values that are also used in the box model from Hofmann et al., 2017). It should be noted that in this analysis we are changing not only the time and/or space dependency of  $\Delta^{17}\text{O}_{\text{soil}}$  and  $\Delta^{17}\text{O}_{\text{leaf}}$  but also their global average value. In the base model run the global mean values are  $\Delta^{17}\text{O}_{\text{soil}} = -10.2$  per meg and  $\lambda_{\text{transp}} = 0.5160$ . Table 3 shows that changing to a constant  $\Delta^{17}\text{O}_{\text{soil}} = -5$  per meg has a small effect on global mean  $\Delta^{17}\text{O}$  in atmospheric  $\text{CO}_2$ , whereas using a constant  $\lambda_{\text{transp}} = 0.5160$  results in a decrease of 5.1 per meg in global mean  $\Delta^{17}\text{O}$ . Finally, we see that changing the soil water signature to  $\Delta^{17}\text{O}_{\text{soil}} = -5$  per meg leads to decreases in both the North–South difference and the amplitude of global  $\Delta^{17}\text{O}$ . In Figure S7 of the supporting information we show the annual mean difference of  $\Delta^{17}\text{O}$  for the TM5 simulations with modifications in the water signatures relative to the base model run.

The effect of a change in the global magnitude and the spatial distribution of the soil invasion flux can also be seen in Table 3. An increase from the base value of 30 to 240 PgC/year or even 450 PgC/year leads to a decrease in the global mean  $\Delta^{17}\text{O}$  signature of atmospheric  $\text{CO}_2$ , where the magnitude of the  $\Delta^{17}\text{O}$  drop also depends on the spatial distribution of the soil invasion flux. For respiration scaling (BASE, RESP\_240, and RESP\_450) the soil invasion fluxes are mostly present in the tropical region, whereas for hydrogen scaling (HYD\_240 and HYD\_450) the soil invasion fluxes extend to higher latitudes, which have a lower  $\Delta^{17}\text{O}_{\text{soil}}$  signature and hence result in a lower  $\Delta^{17}\text{O}$  for atmospheric  $\text{CO}_2$ . Also, we see in Table 3 that increasing the soil invasion fluxes leads to a small decrease in the amplitude of global and hemispheric  $\Delta^{17}\text{O}$ . In Figure S8

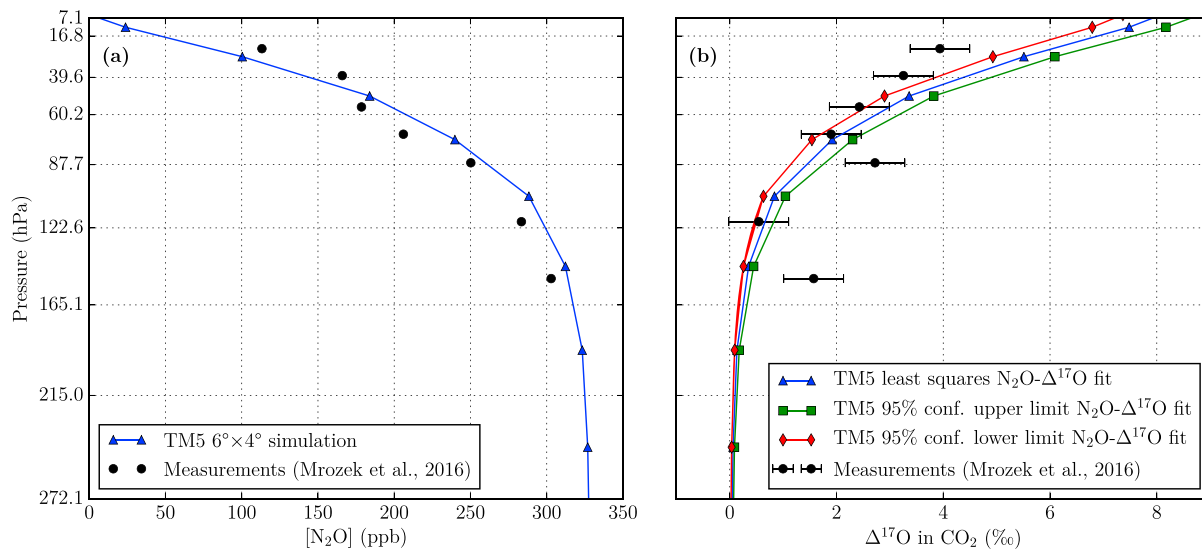


**Figure 10.** Comparison of vertical profiles measured over Sodankylä (67.35°N, 26.93°E; Mrozek et al., 2016) with TM5 model simulations with horizontal resolution of 6° × 4° and with 25 vertical levels. The ticks on the vertical axis coincide with the cell boundaries in the TM5 model with 25 vertical levels. (a) Stratospheric profile of N<sub>2</sub>O mole fraction. (b) Stratospheric profile of Δ<sup>17</sup>O in CO<sub>2</sub> compared with TM5 least squares N<sub>2</sub>O-Δ<sup>17</sup>O fit simulation (BASE), 95% confidence upper limit fit simulation (ST\_UPPER) and 95% confidence lower limit fit simulation (ST\_LOWER).

of the supporting information we show the global mean Δ<sup>17</sup>O distribution for changes in the soil invasion fluxes.

Finally, we show in Table 3 that incorporating the CO + OH reaction with the enrichment  $\epsilon_{\text{CO+OH}}$  from Röckmann et al. (1998a) (CO\_ROCK) has a small positive effect on the resulting Δ<sup>17</sup>O of atmospheric CO<sub>2</sub>, whereas a larger negative effect was found for the fractionation factors from Feilberg et al. (2005) (CO\_FEIL). Based on the enrichment coefficients given in section 2.4.2, we expect that more <sup>18</sup>O-enriched CO<sub>2</sub> is produced in CO\_FEIL than for CO\_ROCK, which explains its lower resulting Δ<sup>17</sup>O signature in atmospheric CO<sub>2</sub>. Because the coefficients from Röckmann et al. (1998a) were also used to produce the CO isotopologue fields by Gromov (2013), we consider the results for CO\_ROCK to be most representative. In Figure S9 of the supporting information we show the distribution of the annual mean anomalies for the calculated Δ<sup>17</sup>O relative to the base model run.

### 3.2. Local Model Simulations

#### 3.2.1. Model-Measurement Comparisons

To test the ability of our model to simulate Δ<sup>17</sup>O in atmospheric CO<sub>2</sub>, we compare our model results with a stratospheric profile measured above Sodankylä, Finland (Mrozek et al., 2016) and with tropospheric measurement series for Göttingen, Germany (Hofmann et al., 2017) and Taipei, Taiwan (Liang et al., 2017b). We selected these two data sets, because the measurement periods overlap (partially) with our model output for years 2010–2014. It should be noted that we are using a relatively coarse resolution for our model (a 6° × 4° horizontal resolution and 25 vertical levels) and that the model output are daily averages and therefore not fully representative for the observations.

In Figure 10, our TM5 model results are shown alongside the N<sub>2</sub>O mole fraction and Δ<sup>17</sup>O in CO<sub>2</sub> profiles that were obtained from an AirCore with Stratospheric Air Sub-sampler by Mrozek et al. (2016) above Sodankylä, Finland (67.35°N, 26.93°E) on 5 November 2014. Note that the N<sub>2</sub>O mole fractions that are reported by Mrozek et al. (2016) are not directly measured but inferred from measurements of CH<sub>4</sub>. The profile of N<sub>2</sub>O mole fractions from our simulation agrees reasonably well with the “measured” N<sub>2</sub>O profile. Contrary to the measured Δ<sup>17</sup>O in CO<sub>2</sub> signatures, the simulated profile shows a monotonic increase with altitude. For the two observations at highest altitudes (at 24 and 39 hPa) we find that the simulated N<sub>2</sub>O is too low and that the simulated Δ<sup>17</sup>O in CO<sub>2</sub> is too high, which suggests that the sampled air is younger than simulated in the transport model for these altitudes. The opposite is found for two of the three lowest observations (at 87 and 151 hPa) indicating that the sampled air was older than the simulated air. Note

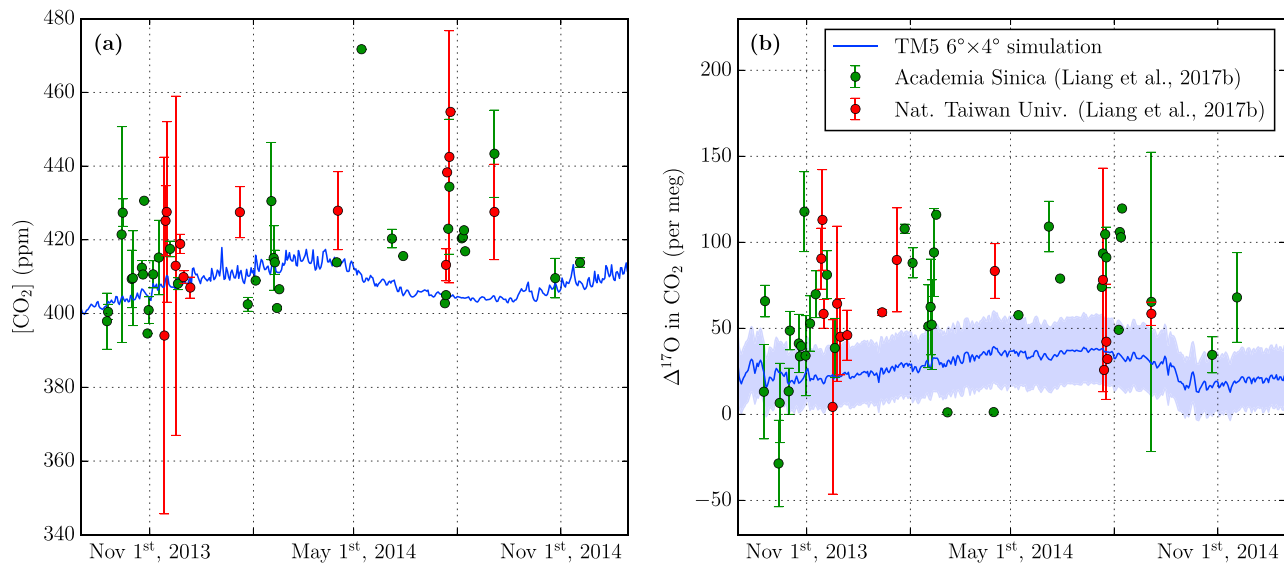


**Figure 11.** Comparison of tropospheric measurements for the Academia Sinica campus (25.04°N, 121.61°E) and the National Taiwan University (25.01°N, 121.54°E) in Taipei, Taiwan, from Liang et al. (2017b) with daily model predictions for the lowest 35 m from TM5 with horizontal resolution of 6° × 4° and 25 vertical levels. (a) CO<sub>2</sub> mixing ratios. (b) Δ<sup>17</sup>O in CO<sub>2</sub>. The shading indicates the spread in model estimates for the 95% confidence interval for the N<sub>2</sub>O-Δ<sup>17</sup>O fit for stratospheric CO<sub>2</sub> (obtained from simulations ST\_LOWER and ST\_UPPER).

that the comparison of our model results with the data from Mrozek et al. (2016) is independent, since the experimental data from Mrozek et al. (2016) were not used as input for the N<sub>2</sub>O-Δ<sup>17</sup>O fit.

In Hofmann et al. (2017), model predictions from an early version of our model (see section S2 of the supporting information for an overview of the differences with our current model) were compared with measurements of Δ<sup>17</sup>O in CO<sub>2</sub> for Göttingen (51.56°N, 9.95°E) and Mt. Brocken (51.80°N, 10.62°E). We have repeated the analysis with our updated model and again find that there is a seasonal cycle in Δ<sup>17</sup>O that is driven by the biosphere. Also, we again find that our model does not show the significant drop in Δ<sup>17</sup>O that is reported based on observations (respectively a mean Δ<sup>17</sup>O of −12.8 and −108.2 per meg before and after 1 July 2011). This unexplained, large drop in the reported observations is discussed in more detail in section 6.2 of Hofmann et al. (2017). A comparison of the measured CO<sub>2</sub> mole fraction and its Δ<sup>17</sup>O signature for Göttingen (51.56°N, 9.95°E) and Mt. Brocken (51.80°N, 10.62°E) with model predictions for the lowest level in TM5 (lowest ~35 m) is given in Figure S10 of the supporting information.

We also compare our model predictions for Δ<sup>17</sup>O in tropospheric CO<sub>2</sub> with measurement data obtained at the Academia Sinica campus (25.04°N, 121.61°E) and the National Taiwan University (25.01°N, 121.54°E) in Taipei, Taiwan, from Liang et al. (2017b). In Figure 11 we compare the measured and simulated CO<sub>2</sub> mole fractions and the Δ<sup>17</sup>O signature. The uncertainty bar that is associated with the measured CO<sub>2</sub> mole fractions is determined from the deviation between measurements taken at different times on the same day, showing the importance of local contributions and the development of the atmospheric boundary layer. The shading in Figure 11b indicates the spread related to the 95% confidence interval for the N<sub>2</sub>O-Δ<sup>17</sup>O(CO<sub>2</sub>) coefficients (slope and offset) that is used in the stratospheric module. The spread in model predictions for the different representations of the stratospheric source is substantial (~40 per meg range) but cannot fully explain the model-measurement discrepancy for this location. Compared to Göttingen, there is a smaller contribution of the biospheric fluxes since Taipei is surrounded by ocean. In addition, we expect a lower seasonality of the biosphere at the latitude of Taipei compared to Göttingen. Contrary to measurement series from Göttingen, our model predictions are lower (mean value of 31.1 per meg) than the Δ<sup>17</sup>O measurements from Taipei (mean value of 58.7 per meg).

### 3.2.2. Future Measurements

The currently available measurement series for Δ<sup>17</sup>O of tropospheric CO<sub>2</sub> have in common that the air was collected in the vicinity of the research groups that performed the measurements. Our objective here is to make use of our 3-D model predictions to identify locations for which measurements of Δ<sup>17</sup>O in CO<sub>2</sub> would be valuable for a better understanding of the global budget of Δ<sup>17</sup>O in CO<sub>2</sub> and further model development.

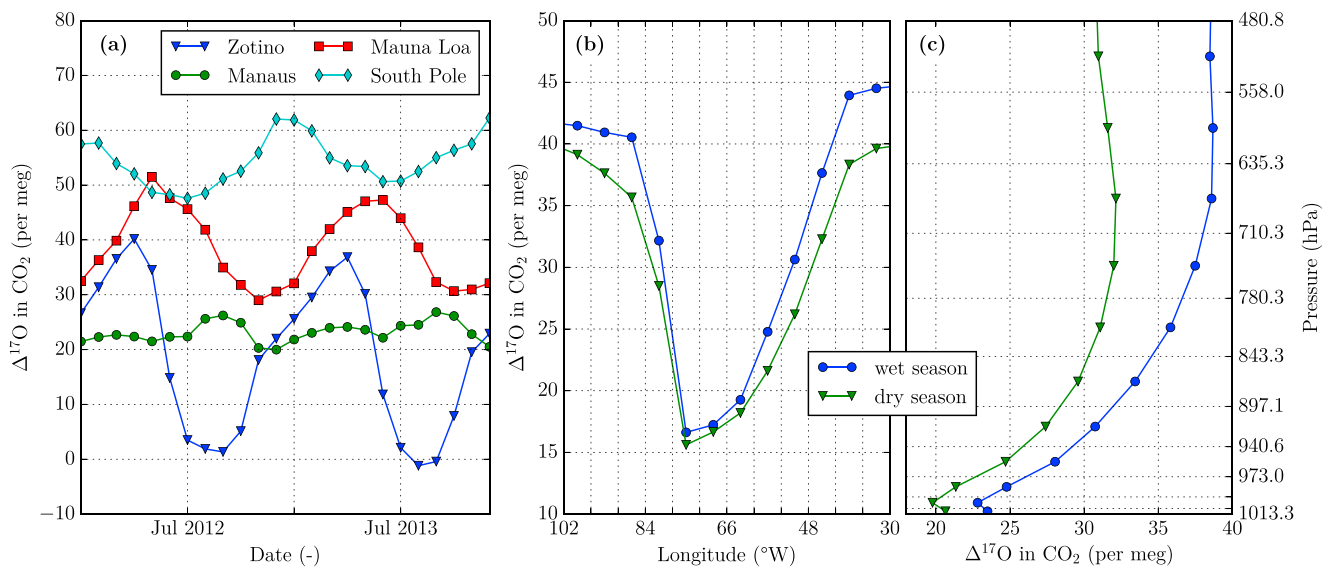


**Figure 12.** TM5 model predictions for  $\Delta^{17}\text{O}$  in atmospheric  $\text{CO}_2$  using base model settings with a horizontal resolution of  $6^\circ \times 4^\circ$  and with 25 vertical levels for selected locations. (a) Time series of  $\Delta^{17}\text{O}$  in  $\text{CO}_2$  for the lowest 500 m of the atmosphere for Zotino ( $60.80^\circ\text{N}$ ,  $89.35^\circ\text{E}$ ), Mauna Loa ( $19.54^\circ\text{N}$ ,  $155.58^\circ\text{W}$ ), Manaus ( $2.15^\circ\text{S}$ ,  $59.00^\circ\text{W}$ ), and South Pole ( $90^\circ\text{S}$ ). (b) Longitudinal cross section through Manaus of  $\Delta^{17}\text{O}$  in  $\text{CO}_2$  for the lowest 500 m of the atmosphere in the dry season (defined here as months in the range July to October) and wet season; the vertical grid lines correspond to the longitudinal boundaries of the TM5 grid. (c) Vertical profile over Manaus of  $\Delta^{17}\text{O}$  in  $\text{CO}_2$  in the dry and wet seasons; the horizontal grid lines correspond to the vertical TM5 hybrid sigma-pressure levels.

A global map of the peak-to-peak amplitude of simulated  $\Delta^{17}\text{O}$  in  $\text{CO}_2$  is shown in Figure S11a of the supporting information. We have selected four locations for which we describe the simulated patterns of  $\Delta^{17}\text{O}$  in  $\text{CO}_2$  in more detail.

Figure 12a shows the  $\Delta^{17}\text{O}$  signature for  $\text{CO}_2$  in the lowest 500 m of the atmosphere for a selection of locations. Zotino ( $60.80^\circ\text{N}$ ,  $89.35^\circ\text{E}$ ) is the location of the Zotino Tall Tower Observatory (Heimann et al., 2014), where we expect a seasonal cycle of 36.1 per meg (see also Table 3), which is substantially larger than the measurement uncertainty of currently available measurement techniques (see also section 1). Also, the mean value of  $\Delta^{17}\text{O}$  at Zotino can be used to better constrain the magnitude of soil invasion fluxes (see Table 3). This site was also used in a study of the  $\delta^{18}\text{O}$  in  $\text{CO}_2$  signal by Cuntz et al. (2002).

Mauna Loa ( $19.54^\circ\text{N}$ ,  $155.58^\circ\text{W}$ ) and South Pole ( $90^\circ\text{S}$ ) are background stations that are famous for their long-standing  $\text{CO}_2$  records that are operated by the National Oceanic and Atmospheric Administration and the Scripps Institution of Oceanography. The time series of  $\Delta^{17}\text{O}$  for  $\text{CO}_2$  in the lowest 500 m of the atmosphere (above the local surface) for Mauna Loa and South Pole in Figure 12a exhibit a seasonal cycle in antiphase with each other. Also, South Pole is an interesting location because we expect a high annual mean  $\Delta^{17}\text{O}$  signature. Dry air samples from the South Pole (British Antarctic Survey station) were collected in 2017 and are currently being analyzed for their  $\Delta^{17}\text{O}$  in  $\text{CO}_2$  signatures by the Centre for Isotope Research in Groningen, the Netherlands.

Also, we included model predictions of  $\Delta^{17}\text{O}$  in  $\text{CO}_2$  for Manaus ( $2.15^\circ\text{S}$ ,  $59.00^\circ\text{W}$ ), the location of the Amazon Tall Tower Observatory (Andreae et al., 2015). Although the annual variation of  $\Delta^{17}\text{O}$  in  $\text{CO}_2$  is small in the lowest 500 m of the atmosphere for Manaus, there is a relatively strong gradient for  $\Delta^{17}\text{O}$  in the longitudinal direction across Manaus (Figure 12b) and a strong vertical gradient above Manaus (Figure 12c). Measurements in and around the Amazon region that are ongoing since February 2018 and analyzed at the LaGEE lab in Brazil could show whether these predicted features in the  $\Delta^{17}\text{O}$  distribution can be observed. The zonal mean annual mean vertical profile for  $\Delta^{17}\text{O}$  in  $\text{CO}_2$  as a function of latitude can be seen in Figure S11b of the supporting information.



## 4. Discussion

### 4.1. Possible Improvements of Model for $\Delta^{17}\text{O}$ in $\text{CO}_2$

In this section we discuss some model features that could be added to or improved with respect to our current 3-D model for  $\Delta^{17}\text{O}$  in  $\text{CO}_2$ . In our current model we represent the stratospheric source of  $\Delta^{17}\text{O}$  by simulating  $\text{N}_2\text{O}$  and converting stratospheric  $\text{N}_2\text{O}$  mole fractions into  $\Delta^{17}\text{O}$  signatures based on their observed correlation as described in section 2.2.1. Although we feel that this is a robust and straightforward approach, we generally prefer to simulate the actual physical processes. As more details of the production process are unfolded by the scientific community, we foresee that it becomes more feasible to implement an explicit description of the production of  $\Delta^{17}\text{O}$  in  $\text{CO}_2$  in future model versions.

To calculate the atmosphere leaf fluxes  $F_{\text{AL}}$  and  $F_{\text{LA}}$ , we use GPP from SiBCASA at a 3-hourly temporal resolution and GPP-weighted  $c_i/c_a$  values from SiBCASA at a monthly temporal resolution as described in section 2.3.1. Also, we assume in our current model that leaf respiration is a constant fraction of 12% of GPP, similar to Ciais et al. (1997a). In future studies we intend to use  $c_i/c_a$  values and leaf respiration from SiBCASA at a 3-hourly temporal resolution to be fully consistent with the temporal resolution of GPP. In the comprehensive  $\delta^{18}\text{O}$  model from Cuntz et al. (2003a, 2003b) these components are also simulated at the same temporal resolution.

For some input fields we use year-specific data, such as the meteorological data ERA-Interim (Dee et al., 2011) that drives the atmospheric transport in TM5. Also, the vegetation-atmosphere fluxes from the SiBCASA model are calculated using the ERA-Interim meteorology. For other input fields, we resort to annually repeating fields, such as for the CO isotopologue fields (Gromov, 2013) and the OH fields (Spivakovsky et al., 2000). In general, we preferably use year-specific input data to capture interannual variability of the different processes. Especially for CO oxidation, we expect some interannual variability due to the irregular occurrence of wildfires (which is major source of CO; Holloway et al., 2000) that we are now not able to simulate.

Another possible improvement is the resolution of the transport model for the performed simulations, which is relatively coarse (a horizontal resolution of  $6^\circ \times 4^\circ$  and a vertical resolution of 25 layers). A finer horizontal resolution could lead to better agreement with local surface measurements, and a finer vertical resolution could be more representative for the STE, which is of importance to the  $\Delta^{17}\text{O}$  in  $\text{CO}_2$  budget and its ability to be used as tracer of GPP, as discussed in section 4.3. For follow-up studies focusing on specific regions, we intend to use finer spatial resolutions.

Finally, a valuable extension of this model would be to implement a “tracer tagging” method that allows to disentangle the contributions of different processes (e.g., biosphere exchange or fossil fuel combustion) on the resulting  $\Delta^{17}\text{O}$  signature of  $\text{CO}_2$ . This would allow to effectively attribute the seasonal patterns, interannual variability, or local disturbances that appear in the simulated  $\Delta^{17}\text{O}$  signature to these processes. Such a tracer tagging technique was also used in the  $\delta^{18}\text{O}$  studies from Ciais et al. (1997a, 1997b), Peylin et al. (1997, 1999), and Cuntz et al. (2003a, 2003b) to quantify the contribution of different processes to the simulated  $\delta^{18}\text{O}$  signature for atmospheric  $\text{CO}_2$ .

### 4.2. Required Measurements of $\Delta^{17}\text{O}$ in $\text{CO}_2$

In this section we discuss issues related to the measurements of  $\Delta^{17}\text{O}$  in  $\text{CO}_2$ . For  $\delta^{18}\text{O}$  in  $\text{CO}_2$  there is a vast network of well characterized measurement stations operated by the National Oceanic and Atmospheric Administration (NOAA) and collaborating organizations that measure  $\delta^{18}\text{O}$  in  $\text{CO}_2$  at a regular basis in addition to other atmospheric compounds and meteorological variables. These flasks are typically already collected with dried air, and with new measurement techniques for  $\Delta^{17}\text{O}$  in  $\text{CO}_2$  the air in these flasks is sufficient for a high-precision ( $\pm 20$  per meg) analysis. The opportunity to start a global characterization of actual signatures followed by a monitoring effort across a subset of most interesting sites thus could be seized. In section 3.2.2, we describe in more detail four locations where measurements have, or could be, started using existing resources.

Besides these observations of  $\Delta^{17}\text{O}$  on the global scale that can help to understand the budget of  $\Delta^{17}\text{O}$  in  $\text{CO}_2$ , there is also a need to measure the individual processes that affect  $\Delta^{17}\text{O}$  in  $\text{CO}_2$ . The value of experiments that unravel the remaining uncertainties about the stratospheric production of  $\Delta^{17}\text{O}$  was already mentioned in section 4.1. Also, controlled laboratory measurements on the effect of plant assimilation on the  $\Delta^{17}\text{O}$  signature of atmospheric  $\text{CO}_2$  could be valuable to test the assumptions used in our current model that are

for a large part based on earlier works on  $\delta^{18}\text{O}$  in  $\text{CO}_2$  (e.g., Gillon & Yakir, 2000, 2001). Furthermore, field scale studies can help to quantify the effect of these leaf-scale processes and entrainment on  $\Delta^{17}\text{O}$  in the atmospheric boundary layer (as done for  $\delta^{13}\text{C}$  and  $\delta^{18}\text{O}$  by Vilà-Guerau de Arellano et al., 2019)

#### 4.3. Potential of $\Delta^{17}\text{O}$ in $\text{CO}_2$ as Tracer of GPP

In this final discussion section we reflect on the potential of  $\Delta^{17}\text{O}$  in  $\text{CO}_2$  to function as a tracer of GPP. One of the main requirements for its use as tracer of GPP is that the stratospheric influx of  $\Delta^{17}\text{O}$  in  $\text{CO}_2$  can be quantified accurately. However, as described in section 2.2.3, estimates for the STE vary considerably. Combination with other tracers (e.g.,  $^7\text{Be}$ , as described by Dutkiewicz & Husain, 1985) might be necessary to reduce the uncertainty in STE.

One of the key variables in the budget of  $\Delta^{17}\text{O}$  in  $\text{CO}_2$  is the  $c_i/c_a$  ratio that relates the gross exchange fluxes between atmosphere and leaf to GPP as described in section 2.3.1. Cuntz (2011) pointed out in a commentary about the GPP estimate by Welp et al. (2011) that uncertainty in the  $c_i/c_a$  ratio (or the percentage of the  $\text{CO}_2$  that diffuses into a leaf that is fixed) can have significant effects on the inferred GPP. This exemplifies the necessity to better constrain  $c_i/c_a$ , which might be achieved with  $\delta^{13}\text{C}$  observations (Peters et al., 2018).

Similarly, the large uncertainty in the magnitude of soil invasion fluxes that was reported by Wingate et al. (2009) has implications for the potential use of  $\Delta^{17}\text{O}$  in  $\text{CO}_2$  as a tracer of GPP. If the soil invasion fluxes are underestimated, this could lead to overestimating GPP since these processes have a similar effect on  $\Delta^{17}\text{O}$  in  $\text{CO}_2$ . The ongoing research on carbonic anhydrase in soils from the COS community might also lead to better quantification of the  $\text{CO}_2$  soil invasion fluxes and as such benefit the use of  $\Delta^{17}\text{O}$  in  $\text{CO}_2$  as tracer of GPP.

Finally, we address the effect of the hydrological cycle on the budget of  $\Delta^{17}\text{O}$  in atmospheric  $\text{CO}_2$ . The main reason to explore the use of  $\Delta^{17}\text{O}$  as tracer for GPP instead of  $\delta^{18}\text{O}$  was that  $\Delta^{17}\text{O}$  is hardly sensitive to the hydrological cycle which greatly simplifies its interpretation and modeling according to Hoag et al. (2005). Still, we have put much effort in calculating the  $\Delta^{17}\text{O}$  isotopic composition of different water reservoirs (e.g., soil water and leaf water, as discussed in section 2.3.1) and we find that changing these values can have a significant effect at high northern latitudes, as described in section 3.1.3. Also, a recent study by Tian et al. (2018) shows that  $\Delta^{17}\text{O}$  of precipitation collected at Indianapolis (Indiana, USA), can vary considerably within months. As such, the use of  $\Delta^{17}\text{O}$  in  $\text{CO}_2$  could be more involved than originally envisioned by Hoag et al. (2005) depending on the specifics of the application.

## 5. Conclusions

We developed a 3-D model framework for  $\Delta^{17}\text{O}$  (defined as  $\Delta^{17}\text{O} = \ln(\delta^{17}\text{O} + 1) - \lambda_{\text{RL}} \cdot \ln(\delta^{18}\text{O} + 1)$ , with  $\lambda_{\text{RL}} = 0.5229$ ) in atmospheric  $\text{CO}_2$ , using the terrestrial biosphere model SiBCASA and atmospheric transport model TM5. In our model framework, the stratospheric source of  $\Delta^{17}\text{O}$  in  $\text{CO}_2$  is based on the observed  $\text{N}_2\text{O}$ – $\Delta^{17}\text{O}$  correlation using available stratospheric data. We included the  $\text{CO}_2$  exchange fluxes from biosphere, oceans, and soils with the atmosphere. Also, we added the release of  $\text{CO}_2$  to the atmosphere from fossil fuel combustion and biomass burning and the production of  $\text{CO}_2$  through the oxidation of atmospheric CO.

Our 3-D model (with base model settings) predicts an average  $\Delta^{17}\text{O}$  signature of 39.6 per meg for  $\text{CO}_2$  in the lowest 500 m of the atmosphere, which is roughly 20 per meg lower than the prediction from the box model by Hofmann et al. (2017). This difference can be attributed mostly to the larger biosphere-atmosphere exchange in the 3-D model (global mean  $F_{\text{AL}} = -514.5 \text{ PgC/year}$  for 2012/2013) compared to the box model ( $F_{\text{AL}} = -352 \text{ PgC/year}$ ) by Hofmann et al. (2017). For the NH and SH we predict a mean  $\Delta^{17}\text{O}$  signature of 31.6 and 47.6 per meg, respectively. In addition, the  $\Delta^{17}\text{O}$  signature exhibits a seasonal cycle with a peak-to-peak amplitude of 17.7 for the NH and 5.1 per meg for the SH, showing the largest drop in  $\Delta^{17}\text{O}$  during the respective summer months for both hemispheres.

We showed that  $\Delta^{17}\text{O}$  model predictions are sensitive to changes in the coefficients describing the  $\text{N}_2\text{O}$ – $\Delta^{17}\text{O}$  correlation for stratospheric  $\text{CO}_2$ . Also, the magnitude and spatial distribution of the soil invasion fluxes have a significant effect on  $\Delta^{17}\text{O}$  in atmospheric  $\text{CO}_2$ . Furthermore, it was found that using a spatially explicit soil water signature  $\Delta^{17}\text{O}_{\text{soil}}$  and time- and space-dependent leaf water signature  $\Delta^{17}\text{O}_{\text{leaf}}$  has a limited effect on the resulting  $\Delta^{17}\text{O}$  in atmospheric  $\text{CO}_2$  and that the oxidation of CO has a minor effect on  $\Delta^{17}\text{O}$  in atmospheric  $\text{CO}_2$ .

We compared our model predictions with a stratospheric profile of  $\Delta^{17}\text{O}$  in  $\text{CO}_2$  measured above Sodankylä, Finland (Mrozek et al., 2016), which showed good agreement indicating that our 3-D model is able to simulate these large-scale features of  $\Delta^{17}\text{O}$  in atmospheric  $\text{CO}_2$ . Comparisons of model predictions with currently available tropospheric measurements of  $\Delta^{17}\text{O}$  in  $\text{CO}_2$  remain inconclusive due to the unexpected interannual variability for measurements from Göttingen, Germany (Hofmann et al., 2017) and the influence of local disturbances that cannot be resolved in our global model for Taipei, Taiwan (Liang & Mahata, 2015).

We identified Zotino, Russia (60.80°N, 89.35°E) as a suitable location to detect a large seasonal cycle of  $\Delta^{17}\text{O}$  in  $\text{CO}_2$  of 36.1 per meg, which is substantially larger than the uncertainty of several recently developed measurement techniques for  $\Delta^{17}\text{O}$  in  $\text{CO}_2$ . Mauna Loa, USA (19.54°N, 155.58°W) and South Pole (90°S) are suitable background locations for which we predict a mean  $\Delta^{17}\text{O}$  in  $\text{CO}_2$  of 36.2 and 52.5 per meg respectively. For Manaus, Brazil (2.15°S, 59.00°W) we predict a small seasonal cycle in  $\Delta^{17}\text{O}$  in  $\text{CO}_2$  of 2.9 per meg but a strong vertical and longitudinal gradient. Measurements at the suggested locations or at comparable sites could help to further increase our understanding of the global  $\Delta^{17}\text{O}$  budget for tropospheric  $\text{CO}_2$ .

### Acknowledgments

We thank Thomas Launois for providing  $\text{H}_2$  deposition maps. The European Research Council (ERC) is acknowledged for funding this research (649087) as part of the ASICA (Airborne Stable Isotopes of Carbon from the Amazon) project. The model simulations in this work have been performed using a grant for computing time (SH-312-14) from the Netherlands Organization for Scientific Research (NWO). The model output data that are used to produce the figures and tables in this paper are hosted by the ICOS Carbon Portal and are accessible online (<https://doi.org/10.18160/3D4N-5YMF>). We thank Kristie Boering and two anonymous reviewers for their constructive suggestions.

### References

- Adnew, G. A., Hofmann, M. E. G., Paul, D., Laskar, A., Surma, J., Albrecht, N., et al. (2019). Determination of the triple oxygen and carbon isotopic composition of  $\text{CO}_2$  from atomic ion fragments formed in the ion source of the 253 Ultra High-Resolution Isotope Ratio Mass Spectrometer. *Rapid Communications in Mass Spectrometry*. <https://doi.org/10.1002/rcm.8478>
- Affolter, S., Häuselmann, A. D., Fleitmann, D., Häuselmann, P., & Leuenberger, M. (2015). Triple isotope ( $\delta\text{D}$ ,  $\delta^{17}\text{O}$ ,  $\delta^{18}\text{O}$ ) study on precipitation, drip water and speleothem fluid inclusions for a Western Central European cave (NW Switzerland). *Quaternary Science Reviews*, 127, 73–89. <https://doi.org/10.1016/j.quascirev.2015.08.030>
- Alexander, B., Vollmer, M. K., Jackson, T., Weiss, R. F., & Thiemens, M. H. (2001). Stratospheric  $\text{CO}_2$  isotopic anomalies and  $\text{SF}_6$  and CFC tracer concentrations in the Arctic polar vortex. *Geophysical Research Letters*, 28(21), 4103–4106. <https://doi.org/10.1029/2001GL013692>
- Andreae, M. O., Acevedo, O. C., Araújo, A., Artaxo, P., Barbosa, C. G. G., Barbosa, H. M. J., et al. (2015). The Amazon Tall Tower Observatory (ATTO): Overview of pilot measurements on ecosystem ecology, meteorology, trace gases, and aerosols. *Atmospheric Chemistry and Physics*, 15(18), 10,723–10,776. <https://doi.org/10.5194/acp-15-10723-2015>
- Appenzeller, C., Holton, J. R., & Rosenlof, K. H. (1996). Seasonal variation of mass transport across the tropopause. *Journal of Geophysical Research*, 101(D10), 15,071–15,078. <https://doi.org/10.1029/96JD00821>
- Assonov, S. S., & Brenninkmeijer, C. A. M. (2003). A redetermination of absolute values for  $^{17}\text{RVPDB-CO}_2$  and  $^{17}\text{RVSMOW}$ . *Rapid Communications in Mass Spectrometry*, 17(10), 1017–1029. <https://doi.org/10.1002/rcm.1011>
- Assonov, S. S., Brenninkmeijer, C. A. M., Schuck, T., & Umezawa, T. (2013).  $\text{N}_2\text{O}$  as a tracer of mixing stratospheric and tropospheric air based on CARIBIC data with applications for  $\text{CO}_2$ . *Atmospheric Environment*, 79, 769–779. <https://doi.org/10.1016/j.atmosenv.2013.07.035>
- Baertschi, P. (1976). Absolute  $^{18}\text{O}$  content of standard mean ocean water. *Earth and Planetary Science Letters*, 31(3), 341–344. [https://doi.org/10.1016/0012-821X\(76\)90115-1](https://doi.org/10.1016/0012-821X(76)90115-1)
- Barkan, E., & Luz, B. (2012). High-precision measurements of  $^{17}\text{O}/^{16}\text{O}$  and  $^{18}\text{O}/^{16}\text{O}$  ratios in  $\text{CO}_2$ . *Rapid Communications in Mass Spectrometry*, 26(23), 2733–2738. <https://doi.org/10.1002/rcm.6400>
- Beer, C., Reichstein, M., Tomelleri, E., Ciais, P., Jung, M., Carvalhais, N., et al. (2010). Terrestrial gross carbon dioxide uptake: Global distribution and covariation with climate. *Science*, 329(5993), 834–838. <https://doi.org/10.1126/science.1184984>
- Bergamaschi, P., Corazza, M., Karstens, U., Athanassiadou, M., Thompson, R. L., Pison, I., et al. (2015). Top-down estimates of European  $\text{CH}_4$  and  $\text{N}_2\text{O}$  emissions based on four different inverse models. *Atmospheric Chemistry and Physics*, 15(2), 715–736. <https://doi.org/10.5194/acp-15-715-2015>
- Boering, K. A., Jackson, T., Hoag, K. J., Cole, A. S., Perri, M. J., Thiemens, M., & Atlas, E. (2004). Observations of the anomalous oxygen isotopic composition of carbon dioxide in the lower stratosphere and the flux of the anomaly to the troposphere. *Geophysical Research Letters*, 31, L03109. <https://doi.org/10.1029/2003GL018451>
- Bönisch, H., Hoor, P., Gurk, C., Feng, W., Chipperfield, M., Engel, A., & Bregman, B. (2008). Model evaluation of  $\text{CO}_2$  and  $\text{SF}_6$  in the extratropical UT/LS region. *Journal of Geophysical Research*, 113, D06101. <https://doi.org/10.1029/2007JD008829>
- Booth, B. B. B., Jones, C. D., Collins, M., Totterdell, I. J., Cox, P. M., Sitch, S., et al. (2012). High sensitivity of future global warming to land carbon cycle processes. *Environmental Research Letters*, 7(2), 024002. <https://doi.org/10.1088/1748-9326/7/2/024002>
- Bowen, G. J., & Revenaugh, J. (2003). Interpolating the isotopic composition of modern meteoric precipitation. *Water Resources Research*, 39(10), 1299. <https://doi.org/10.1029/2003WR002086>
- Bregman, B., Meijer, E., & Scheele, R. (2006). Key aspects of stratospheric tracer modeling using assimilated winds. *Atmospheric Chemistry and Physics*, 6(12), 4529–4543. <https://doi.org/10.5194/acp-6-4529-2006>
- Brenninkmeijer, C. A. M., Kraft, P., & Mook, W. G. (1983). Oxygen isotope fractionation between  $\text{CO}_2$  and  $\text{H}_2\text{O}$ . *Chemical Geology*, 41, 181–190. [https://doi.org/10.1016/S0009-2541\(83\)80015-1](https://doi.org/10.1016/S0009-2541(83)80015-1)
- Brenninkmeijer, C. A. M., Röckmann, T., Bräunlich, M., Jöckel, P., & Bergamaschi, P. (1999). Review of progress in isotope studies of atmospheric carbon monoxide. *Chemosphere - Global Change Science*, 1(1-3), 33–52. [https://doi.org/10.1016/S1465-9972\(99\)00018-5](https://doi.org/10.1016/S1465-9972(99)00018-5)
- Brühl, C., Steil, B., Stiller, G., Funke, B., & Jöckel, P. (2007). Nitrogen compounds and ozone in the stratosphere: Comparison of MIPAS satellite data with the chemistry climate model ECHAM5/MESSEy1. *Atmospheric Chemistry and Physics*, 7(21), 5585–5598. <https://doi.org/10.5194/acp-7-5585-2007>
- Chakraborty, S., & Bhattacharya, S. K. (2003). Experimental investigation of oxygen isotope exchange between  $\text{CO}_2$  and  $\text{O}(^1\text{D})$  and its relevance to the stratosphere. *Journal of Geophysical Research*, 108(D23), 4724. <https://doi.org/10.1029/2002JD002915>
- Ciais, P., Denning, A. S., Tans, P. P., Berry, J. A., Randall, D. A., Collatz, G. J., et al. (1997a). A three-dimensional synthesis study of  $\delta^{18}\text{O}$  in atmospheric  $\text{CO}_2$ : 1. Surface fluxes. *Journal of Geophysical Research*, 102(D5), 5857–5872. <https://doi.org/10.1029/96JD02360>

- Ciais, P., Tans, P. P., Denning, A. S., Francey, R. J., Troler, M., Meijer, H. A. J., et al. (1997b). A three-dimensional synthesis study of  $\delta^{18}\text{O}$  in atmospheric  $\text{CO}_2$ : 2. Simulations with the TM2 transport model. *Journal of Geophysical Research*, 102(D5), 5873–5883. <https://doi.org/10.1029/96JD02361>
- Collatz, G. J., Ball, J. T., Grivet, C., & Berry, J. A. (1991). Physiological and environmental regulation of stomatal conductance, photosynthesis and transpiration: A model that includes a laminar boundary layer. *Agricultural and Forest Meteorology*, 54(2–4), 107–136. [https://doi.org/10.1016/0168-1923\(91\)90002-8](https://doi.org/10.1016/0168-1923(91)90002-8)
- Collatz, G. J., Ribas-Carbo, M., & Berry, J. A. (1992). Coupled photosynthesis-stomatal conductance model for leaves of  $\text{C}_4$  plants. *Australian Journal of Plant Physiology*, 19(5), 519. <https://doi.org/10.1071/PP9920519>
- Corazza, M., Bergamaschi, P., Vermeulen, A. T., Aalto, T., Haszpra, L., Meinhardt, F., et al. (2011). Inverse modelling of European  $\text{N}_2\text{O}$  emissions: Assimilating observations from different networks. *Atmospheric Chemistry and Physics*, 11(5), 2381–2398. <https://doi.org/10.5194/acp-11-2381-2011>
- Cuntz, M. (2011). A dent in carbon's gold standard. *Nature*, 477(7366), 547–548. <https://doi.org/10.1038/477547a>
- Cuntz, M., Ciais, P., & Hoffmann, G. (2002). Modelling the continental effect of oxygen isotopes over Eurasia. *Tellus B*, 54(5), 895–911. <https://doi.org/10.1034/j.1600-0889.2002.01341.x>
- Cuntz, M., Ciais, P., Hoffmann, G., Allison, C. E., Francey, R. J., Knorr, W., et al. (2003a). A comprehensive global three-dimensional model of  $\delta^{18}\text{O}$  in atmospheric  $\text{CO}_2$ : 2. Mapping the atmospheric signal. *Journal of Geophysical Research*, 108(D17), 4528. <https://doi.org/10.1029/2002JD003154>
- Cuntz, M., Ciais, P., Hoffmann, G., & Knorr, W. (2003b). A comprehensive global three-dimensional model of  $\delta^{18}\text{O}$  in atmospheric  $\text{CO}_2$ : 1. Validation of surface processes. *Journal of Geophysical Research*, 108(D17), 4527. <https://doi.org/10.1029/2002JD003153>
- DeMore, W. B., Sander, S. P., Golden, D. M., Hampson, R. F., Kurylo, M. J., Howard, C. J., et al. (1997). Chemical kinetics and photochemical data for use in stratospheric modeling (Evaluation Number 12, Tech. Rep.): Jet Propulsion Laboratory Pasadena California.
- Dee, D. P., Uppala, S. M., Simmons, A. J., Berrisford, P., Poli, P., Kobayashi, S., et al. (2011). The ERA-Interim reanalysis: Configuration and performance of the data assimilation system. *Quarterly Journal of the Royal Meteorological Society*, 137(656), 553–597. <https://doi.org/10.1002/qj.828>
- Dubey, M. K., Mohrslad, R., Donahue, N. M., & Anderson, J. G. (1997). Isotope specific kinetics of hydroxyl radical (OH) with water ( $\text{H}_2\text{O}$ ): Testing models of reactivity and atmospheric fractionation. *The Journal of Physical Chemistry A*, 101(8), 1494–1500. <https://doi.org/10.1021/jp962332p>
- Dutkiewicz, V. A., & Husain, L. (1985). Stratospheric and tropospheric components of  $^7\text{Be}$  in surface air. *Journal of Geophysical Research*, 90(D3), 5783. <https://doi.org/10.1029/JD090iD03p05783>
- Eiler, J. M., & Schauble, E. (2004).  $^{18}\text{O}^{13}\text{C}^{16}\text{O}$  in Earth's atmosphere. *Geochimica et Cosmochimica Acta*, 68(23), 4767–4777. <https://doi.org/10.1016/j.gca.2004.05.035>
- Farquhar, G. D., Lloyd, J., Taylor, J. A., Flanagan, L. B., Syvertsen, J. P., Hubick, K. T., et al. (1993). Vegetation effects on the isotope composition of oxygen in atmospheric  $\text{CO}_2$ . *Nature*, 363(6428), 439–443. <https://doi.org/10.1038/363439a0>
- Farquhar, G. D., von Caemmerer, S., & Berry, J. A. (1980). A biochemical model of photosynthetic  $\text{CO}_2$  assimilation in leaves of  $\text{C}_3$  species. *Planta*, 149(1), 78–90. <https://doi.org/10.1007/BF00386231>
- Feilberg, K. L., Johnson, M. S., & Nielsen, C. J. (2005). Relative rates of reaction of  $^{13}\text{C}^{16}\text{O}$ ,  $^{12}\text{C}^{18}\text{O}$ ,  $^{12}\text{C}^{17}\text{O}$  and  $^{13}\text{C}^{18}\text{O}$  with OH and OD radicals. *Physical Chemistry Chemical Physics*, 7(11), 2318. <https://doi.org/10.1039/b503350k>
- Feilberg, K. L., Sellevåg, S. R., Nielsen, C. J., Griffith, D. W. T., & Johnson, M. S. (2002).  $\text{CO} + \text{OH} \rightarrow \text{CO}_2 + \text{H}$ : The relative reaction rate of five CO isotopologues. *Physical Chemistry Chemical Physics*, 4(19), 4687–4693. <https://doi.org/10.1039/B204827M>
- Francey, R. J., & Tans, P. P. (1987). Latitudinal variation in oxygen-18 of atmospheric  $\text{CO}_2$ . *Nature*, 327(6122), 495–497. <https://doi.org/10.1038/327495a0>
- Giglio, L., Randerson, J. T., & van der Werf, G. R. (2013). Analysis of daily, monthly, and annual burned area using the fourth-generation global fire emissions database (GFED4). *Journal of Geophysical Research: Biogeosciences*, 118, 317–328. <https://doi.org/10.1002/jgrg.20042>
- Gillon, J. S., & Yakir, D. (2000). Naturally low carbonic anhydrase activity in  $\text{C}_4$  and  $\text{C}_3$  plants limits discrimination against  $\text{C}^{18}\text{O}$  during photosynthesis. *Plant, Cell and Environment*, 23(9), 903–915. <https://doi.org/10.1046/j.1365-3040.2000.00597.x>
- Gillon, J., & Yakir, D. (2001). Influence of carbonic anhydrase activity in terrestrial vegetation on the  $^{18}\text{O}$  content of atmospheric  $\text{CO}_2$ . *Science*, 291(5513), 2584–2587. <https://doi.org/10.1126/science.1056374>
- Gromov, S. S. (2013). Stable isotope composition of atmospheric carbon monoxide: A modelling study (Ph.D. thesis), Johannes Gutenberg-Universität Mainz. <https://doi.org/10.13140/RG.2.2.30769.17760>
- Heimann, M., Schulze, E.-D., Winderlich, J., Andreae, M. O., Chi, X., Gerbig, C., et al. (2014). The Zotino Tall Tower Observatory (ZOTTO): Quantifying large scale biogeochemical changes in Central Siberia. *Nova Acta Leopoldina*, 117(399), 51–64.
- Hirsch, A. I., Michalak, A. M., Bruhwiler, L. M., Peters, W., Dlugokencky, E. J., & Tans, P. P. (2006). Inverse modeling estimates of the global nitrous oxide surface flux from 1998–2001. *Global Biogeochemical Cycles*, 20, GB1008. <https://doi.org/10.1029/2004GB002443>
- Hoag, K. J., Still, C. J., Fung, I. Y., & Boering, K. A. (2005). Triple oxygen isotope composition of tropospheric carbon dioxide as a tracer of terrestrial gross carbon fluxes. *Geophysical Research Letters*, 32, L02802. <https://doi.org/10.1029/2004GL021011>
- Hofmann, M. E. G., Horváth, B., Schneider, L., Peters, W., Schützenmeister, K., & Pack, A. (2017). Atmospheric measurements of  $\Delta^{17}\text{O}$  in  $\text{CO}_2$  in Göttingen, Germany reveal a seasonal cycle driven by biospheric uptake. *Geochimica et Cosmochimica Acta*, 199, 143–163. <https://doi.org/10.1016/j.gca.2016.11.019>
- Holloway, T., Levy, H., & Kasibhatla, P. (2000). Global distribution of carbon monoxide. *Journal of Geophysical Research*, 105(D10), 12,123–12,147. <https://doi.org/10.1029/1999JD901173>
- Holton, J. R. (1990). On the global exchange of mass between the stratosphere and troposphere. *Journal of the Atmospheric Sciences*, 47(3), 392–395. [https://doi.org/10.1175/1520-0469\(1990\)047<0392:OTGEOM>2.0.CO;2](https://doi.org/10.1175/1520-0469(1990)047<0392:OTGEOM>2.0.CO;2)
- Horváth, B., Hofmann, M. E. G., & Pack, A. (2012). On the triple oxygen isotope composition of carbon dioxide from some combustion processes. *Geochimica et Cosmochimica Acta*, 95, 160–168. <https://doi.org/10.1016/j.gca.2012.07.021>
- Huff, A. K., & Thiemens, M. H. (1998).  $^{17}\text{O}/^{16}\text{O}$  and  $^{18}\text{O}/^{16}\text{O}$  isotope measurements of atmospheric carbon monoxide and its sources. *Geophysical Research Letters*, 25(18), 3509–3512. <https://doi.org/10.1029/98GL02603>
- Huijnen, V., Williams, J., van Weele, M., van Noije, T., Krol, M., Dentener, F., et al. (2010). The global chemistry transport model TM5: Description and evaluation of the tropospheric chemistry version 3.0. *Geoscientific Model Development*, 3(2), 445–473. <https://doi.org/10.5194/gmd-3-445-2010>
- Jacobson, A. R., Mikaloff Fletcher, S. E., Gruber, N., Sarmiento, J. L., & Gloor, M. (2007). A joint atmosphere-ocean inversion for surface fluxes of carbon dioxide: 1. Methods and global-scale fluxes. *Global Biogeochemical Cycles*, 21, GB1019. <https://doi.org/10.1029/2005GB002556>



- Johnston, J. C., Röckmann, T., & Brenninkmeijer, C. A. M. (2000). CO<sub>2</sub> + O(<sup>1</sup>D) isotopic exchange: Laboratory and modeling studies. *Journal of Geophysical Research*, 105(D12), 15,213–15,229. <https://doi.org/10.1029/2000JD900070>
- Kaiser, J. (2008). Reformulated <sup>17</sup>O correction of mass spectrometric stable isotope measurements in carbon dioxide and a critical appraisal of historic 'absolute' carbon and oxygen isotope ratios. *Geochimica et Cosmochimica Acta*, 72(5), 1312–1334. <https://doi.org/10.1016/j.gca.2007.12.011>
- Kawagucci, S., Tsunogai, U., Kudo, S., Nakagawa, F., Honda, H., Aoki, S., et al. (2008). Long-term observation of mass-independent oxygen isotope anomaly in stratospheric CO<sub>2</sub>. *Atmospheric Chemistry and Physics*, 8(20), 6189–6197. <https://doi.org/10.5194/acp-8-6189-2008>
- Krol, M., Houweling, S., Bregman, B., van den Broek, M., Segers, A., van Velthoven, P., et al. (2005). The two-way nested global chemistry-transport zoom model TM5: Algorithm and applications. *Atmospheric Chemistry and Physics*, 5(2), 417–432. <https://doi.org/10.5194/acp-5-417-2005>
- Lämmerzahl, P., Röckmann, T., Brenninkmeijer, C. A. M., Krankowsky, D., & Mauersberger, K. (2002). Oxygen isotope composition of stratospheric carbon dioxide. *Geophysical Research Letters*, 29(12), 1582. <https://doi.org/10.1029/2001GL014343>
- Landais, A., Barkan, E., Yakir, D., & Luz, B. (2006). The triple isotopic composition of oxygen in leaf water. *Geochimica et Cosmochimica Acta*, 70(16), 4105–4115. <https://doi.org/10.1016/j.gca.2006.06.1545>
- Laskar, A. H., Mahata, S., Bhattacharya, S. K., & Liang, M.-C. (2019). Triple oxygen and clumped isotope compositions of CO<sub>2</sub> in the middle troposphere. *Earth and Space Science*, 6. <https://doi.org/10.1029/2019EA000573>
- Laskar, A. H., Mahata, S., & Liang, M.-C. (2016). Identification of anthropogenic CO<sub>2</sub> using triple oxygen and clumped isotopes. *Environmental Science & Technology*, 50(21), 11,806–11,814. <https://doi.org/10.1021/acs.est.6b02989>
- Launois, T., Peylin, P., Belviso, S., & Poulter, B. (2015). A new model of the global biogeochemical cycle of carbonyl sulfide Part 2: Use of carbonyl sulfide to constrain gross primary productivity in current vegetation models. *Atmospheric Chemistry and Physics*, 15(16), 9285–9312. <https://doi.org/10.5194/acp-15-9285-2015>
- Li, W., Ni, B., Dequ, J., & Qinglian, Z. (1988). Measurement of the absolute abundance of oxygen-17 in V-SMOW. *Chinese Science Bulletin*, 33(19), 1610–1613.
- Liang, M.-C., Blake, G. A., Yung, Y. L., (2008) Seasonal cycle of C<sup>16</sup>O<sup>16</sup>O, C<sup>16</sup>O<sup>17</sup>O, and C<sup>16</sup>O<sup>18</sup>O in the middle atmosphere: Implications for mesospheric dynamics and biogeochemical sources and sinks of CO<sub>2</sub>. *Journal of Geophysical Research*, 113, D12305. <https://doi.org/10.1029/2007JD008392>
- Liang, M.-C., & Mahata, S. (2015). Oxygen anomaly in near surface carbon dioxide reveals deep stratospheric intrusion. *Scientific Reports*, 5(11), 352. <https://doi.org/10.1038/srep11352>
- Liang, M.-C., Mahata, S., Laskar, A. H., & Bhattacharya, S. K. (2017a). Spatiotemporal variability of oxygen isotope anomaly in near surface air CO<sub>2</sub> over urban, semi-urban and ocean areas in and around Taiwan. *Aerosol and Air Quality Research*, 17(3), 706–720. <https://doi.org/10.4209/aaqr.2016.04.0171>
- Liang, M.-C., Mahata, S., Laskar, A. H., Thieme, M. H., & Newman, S. (2017b). Oxygen isotope anomaly in tropospheric CO<sub>2</sub> and implications for CO<sub>2</sub> residence time in the atmosphere and gross primary productivity. *Scientific Reports*, 7(1), 13180. <https://doi.org/10.1038/s41598-017-12774-w>
- Luz, B., & Barkan, E. (2010). Variations of <sup>17</sup>O/<sup>16</sup>O and <sup>18</sup>O/<sup>16</sup>O in meteoric waters. *Geochimica et Cosmochimica Acta*, 74(22), 6276–6286. <https://doi.org/10.1016/j.gca.2010.08.016>
- Luz, B., Barkan, E., Bender, M. L., Thieme, M. H., & Boering, K. A. (1999). Triple-isotope composition of atmospheric oxygen as a tracer of biosphere productivity. *Nature*, 400(6744), 547–550. <https://doi.org/10.1038/22987>
- Lyons, J. R. (2001). Transfer of mass-independent fractionation in ozone to other oxygen-containing radicals in the atmosphere. *Geophysical Research Letters*, 28(17), 3231–3234. <https://doi.org/10.1029/2000GL012791>
- Mahata, S., Bhattacharya, S. K., & Liang, M.-C. (2016b). An improved method of high-precision determination of Δ<sup>17</sup>O of CO<sub>2</sub> by catalyzed exchange with O<sub>2</sub> using hot platinum. *Rapid Communications in Mass Spectrometry*, 30(1), 119–131. <https://doi.org/10.1002/rcm.7423>
- Mahata, S., Bhattacharya, S. K., Wang, C.-H., & Liang, M.-C. (2013). Oxygen isotope exchange between O<sub>2</sub> and CO<sub>2</sub> over hot platinum: An innovative technique for measuring Δ<sup>17</sup>O in CO<sub>2</sub>. *Analytical Chemistry*, 85(14), 6894–6901. <https://doi.org/10.1021/ac4011777>
- Mahata, S., Wang, C.-H., Bhattacharya, S. K., & Liang, M.-C. (2016a). Near surface CO<sub>2</sub> triple oxygen isotope composition. *Terrestrial, Atmospheric and Oceanic Sciences*, 27(1), 99–106. [https://doi.org/10.1016/j.taos.2015.09.16.01\(A\)](https://doi.org/10.1016/j.taos.2015.09.16.01(A))
- McManus, J. B., Nelson, D. D., & Zahniser, M. S. (2015). Design and performance of a dual-laser instrument for multiple isotopologues of carbon dioxide and water. *Optics Express*, 23(5), 6569. <https://doi.org/10.1364/OE.23.006569>
- Mebel, A. M., Hayashi, M., Kislov, V. V., & Lin, S. H. (2004). Theoretical study of oxygen isotope exchange and quenching in the O(<sup>1</sup>D) + CO<sub>2</sub> reaction. *The Journal of Physical Chemistry A*, 108(39), 7983–7994. <https://doi.org/10.1021/jp049315h>
- Miller, J. B., Yakir, D., White, J. W. C., & Tans, P. P. (1999). Measurement of <sup>18</sup>O/<sup>16</sup>O in the soil-atmosphere CO<sub>2</sub> flux. *Global Biogeochemical Cycles*, 13(3), 761–774. <https://doi.org/10.1029/1999GB900028>
- Monge-Sanz, B. M., Chipperfield, M. P., Simmons, A. J., & Uppala, S. M. (2007). Mean age of air and transport in a CTM: Comparison of different ECMWF analyses. *Geophysical Research Letters*, 34, L04801. <https://doi.org/10.1029/2006GL028515>
- Mrozek, D. J. (2017). Measurements and interpretation of oxygen isotopes in stratospheric carbon dioxide (Ph.D. thesis), Utrecht University.
- Mrozek, D. J., van der Veen, C., Hofmann, M. E. G., Chen, H., Kivi, R., Heikkinen, P., & Röckmann, T. (2016). Stratospheric Air Sub-sampler (SAS) and its application to analysis of Δ<sup>17</sup>O(CO<sub>2</sub>) from small air samples collected with an AirCore. *Atmospheric Measurement Techniques*, 9(11), 5607–5620. <https://doi.org/10.5194/amt-9-5607-2016>
- Nelson, D. D., McManus, J. B., Herndon, S. C., Zahniser, M. S., Tuzson, B., & Emmenegger, L. (2008). New method for isotopic ratio measurements of atmospheric carbon dioxide using a 4.3 μm pulsed quantum cascade laser. *Applied Physics B*, 90(2), 301–309. <https://doi.org/10.1007/s00340-007-2894-1>
- Ogée, J., Sauze, J., Kesselmeier, J., Genty, B., Van Diest, H., Launois, T., & Wingate, L. (2016). A new mechanistic framework to predict OCS fluxes from soils. *Biogeosciences*, 13(8), 2221–2240. <https://doi.org/10.5194/bg-13-2221-2016>
- Oort, A. H. (1983). Global atmospheric circulation statistics, 1958–1973. U.S. Department of Commerce National Oceanic and Atmospheric Administration.
- Pearcy, R. W., & Ehleringer, J. (1984). Comparative ecophysiology of C<sub>3</sub> and C<sub>4</sub> plants. *Plant Cell and Environment*, 7(1), 1–13. <https://doi.org/10.1111/j.1365-3040.1984.tb01194.x>
- Peters, W., Jacobson, A. R., Sweeney, C., Andrews, A. E., Conway, T. J., Masarie, K., et al. (2007). An atmospheric perspective on North American carbon dioxide exchange: CarbonTracker. *Proceedings of the National Academy of Sciences*, 104(48), 18,925–18,930. <https://doi.org/10.1073/pnas.0708986104>
- Peters, W., Krol, M. C., van der Werf, G. R., Houweling, S., Jones, C. D., Hughes, J., et al. (2010). Seven years of recent European net terrestrial carbon dioxide exchange constrained by atmospheric observations. *Global Change Biology*, 16(4), 1317–1337. <https://doi.org/10.1111/j.1365-2486.2009.02078.x>



- Peters, W., van der Velde, I. R., van Schaik, E., Miller, J. B., Ciais, P., Duarte, H. F., et al. (2018). Increased water-use efficiency and reduced CO<sub>2</sub> uptake by plants during droughts at a continental scale. *Nature Geoscience*, 11(10), 744–748. <https://doi.org/10.1038/s41561-018-0212-7>
- Peylin, P., Ciais, P., Denning, A. S., Tans, P. P., Berry, J. A., & White, J. W. C. (1999). A 3-dimensional study of  $\delta^{18}\text{O}$  in atmospheric CO<sub>2</sub>: Contribution of different land ecosystems. *Tellus B*, 51(3), 642–667. <https://doi.org/10.1034/j.1600-0889.1999.t01-2-00006.x>
- Peylin, P., Ciais, P., Tans, P. P., Six, K., Berry, J. A., & Denning, A. S. (1997).  $^{18}\text{O}$  in atmospheric CO<sub>2</sub> simulated by a 3-D transport model: A sensitivity study to vegetation and soil fractionation factors. *Physics and Chemistry of the Earth*, 21(5-6), 463–469. [https://doi.org/10.1016/S0079-1946\(97\)81143-3](https://doi.org/10.1016/S0079-1946(97)81143-3)
- Potter, C. S., Randerson, J. T., Field, C. B., Matson, P. A., Vitousek, P. M., Mooney, H. A., & Klooster, S. A. (1993). Terrestrial ecosystem production: A process model based on global satellite and surface data. *Global Biogeochemical Cycles*, 7(4), 811–841. <https://doi.org/10.1029/93GB02725>
- Prather, M. J. (1986). Numerical advection by conservation of second-order moments. *Journal of Geophysical Research*, 91(D6), 6671. <https://doi.org/10.1029/JD091iD06p06671>
- Röckmann, T., Brenninkmeijer, C. A. M., Neeb, P., & Crutzen, P. J. (1998b). Ozonolysis of nonmethane hydrocarbons as a source of the observed mass independent oxygen isotope enrichment in tropospheric CO. *Journal of Geophysical Research*, 103(D1), 1463–1470. <https://doi.org/10.1029/97JD02929>
- Röckmann, T., Brenninkmeijer, C. A. M., Saueressig, G., Bergamaschi, P., Crowley, J. N., Fischer, H., & Crutzen, P. J. (1998a). Mass-independent oxygen isotope fractionation in atmospheric CO as a result of the reaction CO + OH. *Science*, 281(5376), 544–546. <https://doi.org/10.1126/science.281.5376.544>
- Röckmann, T., Jöckel, P., Gros, V., Bräunlich, M., Possnert, G., & Brenninkmeijer, C. A. M. (2002). Using  $^{14}\text{C}$ ,  $^{13}\text{C}$ ,  $^{18}\text{O}$  and  $^{17}\text{O}$  isotopic variations to provide insights into the high northern latitude surface CO inventory. *Atmospheric Chemistry and Physics*, 2(2), 147–159. <https://doi.org/10.5194/acp-2-147-2002>
- Russell, G. L., & Lerner, J. A. (1981). A new finite-differencing scheme for the tracer transport equation. *Journal of Applied Meteorology*, 20(12), 1483–1498. [https://doi.org/10.1175/1520-0450\(1981\)020<1483:ANFDSF>2.0.CO;2](https://doi.org/10.1175/1520-0450(1981)020<1483:ANFDSF>2.0.CO;2)
- Sanhueza, E., Dong, Y., Lobert, J. M., & Crutzen, P. J. (1998). Carbon monoxide uptake by temperate forest soils: The effects of leaves and humus layers. *Tellus B*, 50(1), 51–58. <https://doi.org/10.1034/j.1600-0889.1998.00004.x>
- Schaefer, K., Collatz, G. J., Tans, P., Denning, A. S., Baker, I., Berry, J., et al. (2008). Combined Simple Biosphere/Carnegie-Ames-Stanford Approach terrestrial carbon cycle model. *Journal of Geophysical Research*, 113, G03034. <https://doi.org/10.1029/2007JG000603>
- Schoeberl, M. R., Douglass, A. R., Stolarski, R. S., Pawson, S., Strahan, S. E., & Read, W. (2008). Comparison of lower stratospheric tropical mean vertical velocities. *Journal of Geophysical Research*, 113, D24109. <https://doi.org/10.1029/2008JD010221>
- Shaheen, R., Janssen, C., & Röckmann, T. (2007). Investigations of the photochemical isotope equilibrium between O<sub>2</sub>, CO<sub>2</sub> and O<sub>3</sub>. *Atmospheric Chemistry and Physics*, 7(2), 495–509. <https://doi.org/10.5194/acp-7-495-2007>
- Spivakovsky, C. M., Logan, J. A., Montzka, S. A., Balkanski, Y. J., Foreman-Fowler, M., Jones, D. B. A., et al. (2000). Three-dimensional climatological distribution of tropospheric OH: Update and evaluation. *Journal of Geophysical Research*, 105(D7), 8931–8980. <https://doi.org/10.1029/1999JD901006>
- Stern, L. A., Amundson, R., & Baisden, W. T. (2001). Influence of soils on oxygen isotope ratio of atmospheric CO<sub>2</sub>. *Global Biogeochemical Cycles*, 15(3), 753–759. <https://doi.org/10.1029/2000GB001373>
- Still, C. J., Berry, J. A., Collatz, G. J., & DeFries, R. S. (2003). Global distribution of C<sub>3</sub> and C<sub>4</sub> vegetation: Carbon cycle implications. *Global Biogeochemical Cycles*, 17(1), 1006. <https://doi.org/10.1029/2001GB001807>
- Stoltmann, T., Casado, M., Daëron, M., Landais, A., & Kassi, S. (2017). Direct, precise measurements of isotopologue abundance ratios in CO<sub>2</sub> using molecular absorption spectroscopy: Application to  $\Delta^{17}\text{O}$ . *Analytical Chemistry*, 89(19), 10,129–10,132. <https://doi.org/10.1021/acs.analchem.7b02853>
- Swinbank, R., & O'Neill, A. (1994). A stratosphere-troposphere data assimilation system. *Monthly Weather Review*, 122(4), 686–702. [https://doi.org/10.1175/1520-0493\(1994\)122<0686:ASTDAS>2.0.CO;2](https://doi.org/10.1175/1520-0493(1994)122<0686:ASTDAS>2.0.CO;2)
- Thiemens, M. H., Chakraborty, S., & Jackson, T. L. (2014). Decadal  $\Delta^{17}\text{O}$  record of tropospheric CO<sub>2</sub>: Verification of a stratospheric component in the troposphere. *Journal of Geophysical Research: Atmospheres*, 119, 6221–6229. <https://doi.org/10.1002/2013JD020317>
- Thiemens, M. H., Jackson, T. L., & Brenninkmeijer, C. A. M. (1995b). Observation of a mass independent oxygen isotopic composition in terrestrial stratospheric CO<sub>2</sub>, the link to ozone chemistry, and the possible occurrence in the Martian atmosphere. *Geophysical Research Letters*, 22(3), 255–257. <https://doi.org/10.1029/94GL02996>
- Thiemens, M. H., Jackson, T., Zipf, E. C., Erdman, P. W., & van Egmond, C. (1995a). Carbon dioxide and oxygen isotope anomalies in the mesosphere and stratosphere. *Science*, 270(5238), 969–972. <https://doi.org/10.1126/science.270.5238.969>
- Tian, C., Wang, L., Kaseke, K. F., & Bird, B. W. (2018). Stable isotope compositions ( $\delta^2\text{H}$ ,  $\delta^{18}\text{O}$  and  $\delta^{17}\text{O}$ ) of rainfall and snowfall in the central United States. *Scientific Reports*, 8(1), 6712. <https://doi.org/10.1038/s41598-018-25102-7>
- Uemura, R., Barkan, E., Abe, O., & Luz, B. (2010). Triple isotope composition of oxygen in atmospheric water vapor. *Geophysical Research Letters*, 37, L04402. <https://doi.org/10.1029/2009GL041960>
- van Noije, T. P. C., Eskes, H. J., van Weele, M., & van Velthoven, P. F. J. (2004). Implications of the enhanced Brewer-Dobson circulation in European Centre for Medium-Range Weather Forecasts reanalysis ERA-40 for the stratosphere-troposphere exchange of ozone in global chemistry transport models. *Journal of Geophysical Research*, 109, D19308. <https://doi.org/10.1029/2004JD004586>
- van der Laan-Luijkx, I. T., van der Velde, I. R., van der Veen, E., Tsuruta, A., Stanislawski, K., Babenhauerheide, A., et al. (2017). The CarbonTracker Data Assimilation Shell (CTDAS) v1.0: Implementation and global carbon balance 2001–2015. *Geoscientific Model Development*, 10(7), 2785–2800. <https://doi.org/10.5194/gmd-10-2785-2017>
- van der Velde, I. R., Miller, J. B., Schaefer, K., van der Werf, G. R., Krol, M. C., & Peters, W. (2014). Terrestrial cycling of  $^{13}\text{CO}_2$  by photosynthesis, respiration, and biomass burning in SiBCASA. *Biogeosciences*, 11(23), 6553–6571. <https://doi.org/10.5194/bg-11-6553-2014>
- van der Werf, G. R., Randerson, J. T., Giglio, L., Collatz, G. J., Mu, M., Kasibhatla, P. S., et al. (2010). Global fire emissions and the contribution of deforestation, savanna, forest, agricultural, and peat fires (1997–2009). *Atmospheric Chemistry and Physics*, 10(23), 11,707–11,735. <https://doi.org/10.5194/acp-10-11707-2010>
- Vilà-Guerau de Arellano, J., Koren, G., Ouwersloot, H. G., van der Velde, I., Röckmann, T., & Miller, J. B. (2019). Sub-diurnal variability of the carbon dioxide and water vapor isotopologues at the field observational scale. *Agricultural and Forest Meteorology*, 275, 114–135. <https://doi.org/10.1016/j.agrformet.2019.05.014>
- Vogel, J. C., Grotes, P. M., & Mook, W. G. (1970). Isotopic fractionation between gaseous and dissolved carbon dioxide. *Zeitschrift für Physik A Hadrons and nuclei*, 230(3), 225–238. <https://doi.org/10.1007/BF01394688>

- Volk, C. M., Elkins, J. W., Fahey, D. W., Dutton, G. S., Gilligan, J. M., Loewenstein, M., et al. (1997). Evaluation of source gas lifetimes from stratospheric observations. *Journal of Geophysical Research*, 102(D21), 25,543–25,564. <https://doi.org/10.1029/97JD02215>
- Wanninkhof, R. (1992). Relationship between wind speed and gas exchange over the ocean. *Journal of Geophysical Research*, 97(C5), 7373. <https://doi.org/10.1029/92JC00188>
- Welp, L. R., Keeling, R. F., Meijer, H. A. J., Bollenbacher, A. F., Piper, S. C., Yoshimura, K., et al. (2011). Interannual variability in the oxygen isotopes of atmospheric CO<sub>2</sub> driven by El Niño. *Nature*, 477(7366), 579–582. <https://doi.org/10.1038/nature10421>
- Wen, J., & Thiemens, M. H. (1993). Multi-isotope study of the O(<sup>1</sup>D) + CO<sub>2</sub> exchange and stratospheric consequences. *Journal of Geophysical Research*, 98(D7), 12,801–12,808. <https://doi.org/10.1029/93JD00565>
- West, J. B., Sobek, A., & Ehleringer, J. R. (2008). A simplified GIS approach to modeling global leaf water isoscapes. *PLoS ONE*, 3(6), e2447. <https://doi.org/10.1371/journal.pone.0002447>
- Wiegel, A. A., Cole, A. S., Hoag, K. J., Atlas, E. L., Schauffler, S. M., & Boering, K. A. (2013). Unexpected variations in the triple oxygen isotope composition of stratospheric carbon dioxide. *Proceedings of the National Academy of Sciences*, 110(44), 17,680–17,685. <https://doi.org/10.1073/pnas.1213082110>
- Wingate, L., Ogée, J., Cuntz, M., Genty, B., Reiter, I., Seibt, U., et al. (2009). The impact of soil microorganisms on the global budget of <sup>18</sup>O in atmospheric CO<sub>2</sub>. *Proceedings of the National Academy of Sciences*, 106(52), 22,411–22,415. <https://doi.org/10.1073/pnas.0905210106>
- Yeung, L. Y., Affek, H. P., Hoag, K. J., Guo, W., Wiegel, A. A., Atlas, E. L., et al. (2009). Large and unexpected enrichment in stratospheric <sup>16</sup>O<sup>13</sup>C<sup>18</sup>O and its meridional variation. *Proceedings of the National Academy of Sciences*, 106(28), 11,496–11,501. <https://doi.org/10.1073/pnas.0902930106>
- Young, E. D., Galy, A., & Nagahara, H. (2002). Kinetic and equilibrium mass-dependent isotope fractionation laws in nature and their geochemical and cosmochemical significance. *Geochimica et Cosmochimica Acta*, 66(6), 1095–1104. [https://doi.org/10.1016/S0016-7037\(01\)00832-8](https://doi.org/10.1016/S0016-7037(01)00832-8)
- Yung, Y. L., DeMore, W. B., & Pinto, J. P. (1991). Isotopic exchange between carbon dioxide and ozone via O(<sup>1</sup>D) in the stratosphere. *Geophysical Research Letters*, 18(1), 13–16. <https://doi.org/10.1029/90GL02478>